Modern rates of glacial sediment accumulation along a 15° S-N transect in fjords from the Antarctic Peninsula to southern Chile

Katherine V. Boldt,[1] Charles A. Nittrouer,[1,2] Bernard Hallet,[2] Michele N. Koppes,[3] Brittany K. Forrest,[1] Julia S. Wellner,[4] and John B. Anderson[5]

Received 24 January 2013; revised 5 September 2013; accepted 9 September 2013; published 10 October 2013.

[1] Rates of glacial erosion in temperate climates rank among the highest worldwide, and the sedimentary products of such erosion record climatic and tectonic signals in many glaciated settings, as well as temporal changes in glacier behavior. Glacial sediment yields are expected to decrease with increasing latitude because decreased temperature and meltwater production reduce glacial sliding, erosion, and sediment transfer; however, this expectation lacks a solid supportive database. Herein we present modern ^{210}Pb-derived sediment accumulation rates on decadal to century time scales for 12 fjords spanning 15° of latitude from the Antarctic Peninsula to southern Chile and interpret the results in light of glacimarine sediment accumulation worldwide. ^{210}Pb records from the Antarctic Peninsula show surprisingly steady sediment accumulation throughout the past century at rates of 1–7 mm yr^{-1}, despite rapid warming and glacial retreat. Cores from the South Shetland Islands reveal accelerated sediment accumulation over the past few decades, likely due to changes in the thermal state of the glaciers in this region, which straddles the boundary between subpolar and temperate conditions. In Patagonia and Tierra del Fuego, sediment accumulates faster (11–24 mm yr^{-1}), and previously collected seismic profiles show that rates reach meters per year close to the glacier termini. This increase in sediment accumulation rates with decreasing latitude reflects the gradient from subpolar to temperate climates and is consistent with glacial erosion being much faster in the temperate climate of southern Chile than in the polar climate of the Antarctic Peninsula.

Citation: Boldt, K. V., C. A. Nittrouer, B. Hallet, M. N. Koppes, B. K. Forrest, J. S. Wellner, and J. B. Anderson (2013), Modern rates of glacial sediment accumulation along a 15°S-N transect in fjords from the Antarctic Peninsula to southern Chile, *J. Geophys. Res. Earth Surf.*, *118*, 2072–2088, doi:10.1002/jgrf.20145.

1. Introduction

[2] Glacial erosion and sediment production are of interest to diverse scientific communities concerned with (1) the interaction of climatic, tectonic, and surface processes that influences the evolution of mountain ranges [e.g., *Egholm et al.*, 2009; *Thomson et al.*, 2010] and (2) the interpretation of environmental and tectonic signals archived in sediments produced by glaciers [e.g., *Griffith and Anderson*, 1989; *Domack and McClennen*, 1996; *Michalchuk et al.*, 2009; *Cowan et al.*, 2010; *Koppes et al.*, 2010]. Sediment production from temperate glaciers is among the greatest worldwide [*Hallet et al.*, 1996], demonstrating the efficacy of glaciers in eroding highlands and producing large volumes of sediment [*Koppes and Montgomery*, 2009], which accumulate in nearshore marine environments [e.g., *Jaeger et al.*, 1998; *Jaeger and Nittrouer*, 1999]. For example, the onset of widespread glaciation and concomitant increase in sedimentation induced by a change to a cooler, more variable climate in the late Cenozoic [*Hay et al.*, 1988; *Zhang et al.*, 2001] is often viewed as responsible for the creation of clastic wedges up to 5 km thick on high-latitude continental margins [e.g., *Syvitski*, 1991; *Vorren et al.*, 1991; *Elverhøi et al.*, 1998; *Berger et al.*, 2008].

[3] One objective of contemporary glacimarine research is to understand the fidelity of recent and past climate-change signals preserved in the sedimentary record, and how these records are altered by time and changing boundary conditions [e.g., *Milliken et al.*, 2009; *Koppes et al.*, 2010; *Fernandez et al.*, 2011; *Simms et al.*, 2011]. Climate controls the extent and thermal regime of glaciers, as well as the amount of meltwater produced [e.g., *Griffith and Anderson*, 1989; *DaSilva et al.*, 1997], with increased meltwater generally promoting glacier erosion by reducing the basal effective pressure [e.g., *Cuffey and Paterson*, 2010]. When abundant, glacial meltwater transports the majority of glacially derived sediment to fjords,

[1]School of Oceanography, University of Washington, Seattle, Washington, USA.
[2]Department of Earth and Space Sciences and Quaternary Research Center, University of Washington, Seattle, Washington, USA.
[3]Department of Geography, University of British Columbia, Vancouver, British Columbia, Canada.
[4]Department of Earth and Atmospheric Sciences, University of Houston, Houston, Texas, USA.
[5]Department of Earth Science, Rice University, Houston, Texas, USA.

Corresponding author: K. V. Boldt, School of Oceanography, University of Washington, Box 357940, Seattle, WA 98195, USA. (kboldt@uw.edu)

2169-9003/13/10.1002/jgrf.20145

where most of this sediment remains trapped [e.g., *Powell and Molnia*, 1989; *Cowan and Powell*, 1991; *Hallet et al*., 1996; *Hunter et al*., 1996]. The large meltwater discharge in temperate glacier-marine systems results in proximal rates of sediment accumulation that can reach tens of meters per year [e.g., *Molnia*, 1983; *Cowan and Powell*, 1991]. In colder settings, the production of sediment by glacial erosion is expected to decrease progressively as surface melt vanishes, because little or no water reaches the bed from the glacier surface to facilitate sliding, erosion, and sediment transport. Moreover, significant sediment production likely vanishes as soon as the basal ice temperature drops below the freezing point [e.g., *Cuffey et al*., 1999]. Thus, for polar and subpolar regions, subglacial sediment production and delivery to fjords are both expected to drop with decreasing air temperature, especially as it drops below 0°C [*Griffith and Anderson*, 1989; *Hooke and Elverhøi*, 1996; *Powell et al*., 1996].

[4] An abrupt decrease in sediment accumulation rates from temperate glaciers in Chile to subpolar and polar glaciers along the Antarctic Peninsula has been well recognized and attributed to climatically controlled differences in glacier dynamics [*Harden et al*., 1992; *Domack and McClennen*, 1996; *DaSilva et al*., 1997]. Analyses of continental-margin sediments from this region provide considerable insight into the history of glacial and climate changes over time scales of 10^3 years and longer [e.g., *Domack et al*., 2001; *Anderson et al*., 2002; *Boyd et al*., 2008; *Milliken et al*., 2009; *Simms et al*., 2011; *Majewski et al*., 2012]. In addition, substantial radiochemical work along Antarctic margins provides important biological and sedimentological chronologies from which to examine how modern climate transitions are impacting the sediment record [*Ledford-Hoffman et al*., 1986; *DeMaster et al*., 1991; *Harden et al*., 1992; *Leventer et al*., 1996; *Monien et al*., 2011]. Quantitative definition of modern accumulation rates complements existing measurements of longer-term sediment accumulation in high-latitude environments [*Boyd et al*., 2008; *Milliken et al*., 2009; *Fernandez et al*., 2011] and reveals how recent climate change has affected accumulation rates in the recent glacimarine sedimentary record [e.g., *Gilbert and Domack*, 2003; *Majewski et al*., 2012].

[5] Herein we measure contemporary sediment accumulation rates from 12 fjords along the western side of the Antarctic Peninsula (WAP), the South Shetland Islands, Tierra del Fuego, and the Southern Patagonia ice field (Figure 1a), with sediments derived from diverse glaciers ranging from subpolar to temperate. For each glacier system, we determined accumulation rates within proximal basins in the fjords using ^{210}Pb analyses, which inform us about sediment accumulation over decadal to centennial time scales. Our objectives include: (1) adding to the limited knowledge about recent sediment accumulation in this region [e.g., *Harris et al*., 1999] and determining the signature of recent rapid warming and glacier retreat in the sediment record [*Vaughan et al*., 2003; *Cook et al*., 2005; *Pritchard and Vaughan*, 2007]; (2) comparing sediment accumulation rates among systems across a range of climatic and glaciologic settings, and defining quantitatively the well-recognized general northerly increase in sediment accumulation rates in the Southern Hemisphere [*Harden et al*., 1992; *Domack and McClennen*, 1996; *DaSilva et al*., 1997]; and (3) comparing the rates and modes of deposition in the study region with those measured using similar records in a range of other glacimarine settings [e.g., *Cowan and Powell*, 1991; *Jaeger and Nittrouer*, 1999]. The accumulation rates presented here are the focus of current work to define sediment yields for individual glaciers at the head of each fjord and to compare the empirical yields with the dynamic characteristics of each glacier system; this work is part of a broader study on the factors controlling rates of glacial erosion and sediment accumulation across climatic regimes [*Boyd et al*., 2008; *Milliken et al*., 2009; *Fernandez et al*., 2011].

2. Geographic and Climatic Setting

[6] The sediments analyzed span 15° of latitude from southern Chile to the Antarctic Peninsula (Figure 1a), where the climate varies from the relatively cold and dry setting along the WAP, to a transitional climate in the South Shetland Islands, and to the warm and wet conditions of southern Chile. This transect provides an ideal setting to study the climatic factors influencing modern glacimarine sedimentation because of the substantial ranges of temperature and precipitation that significantly influence glacier thermal regimes, as well as meltwater and sediment production [e.g., *Griffith and Anderson*, 1989].

[7] Climatic conditions along the WAP range from subpolar to polar, but all of our study sites fall within the subpolar regime. Mean temperatures vary from ~0°C in the austral summer to −8 to −11°C in the winter [*King et al*., 2003], and seasonal sea ice forms within the fjords and on the shelf, although the fjords remain free of sea ice for most of the austral summer [*Domack and Ishman*, 1993]. A 50-year temperature record from Faraday Station (65.2°S, 64.3°W), near Beascochea Bay (BSB, Figure 1b), indicates a general warming rate of 5.7 ± 2.0°C per century, the most rapid in Antarctica [*Vaughan et al*., 2003], as well as a statistically significant increase in the number of precipitation days over the same time period [*Turner et al*., 2005]. Approximately 70% of the Antarctic Peninsula surface area north of 70°S experiences occasional to frequent surface melting [*Rau and Braun*, 2002], and the fraction of annual accumulation experiencing melting has increased tenfold in the past ~600 years [*Abram et al*., 2013]. Such melting generally favors sediment production by glacial erosion, as well as sediment transport and release to fjords where the glaciers terminate. The spine of the Antarctic Peninsula, with mountains that rise up to 3500 m above sea level, is heavily glaciated, and many of the glaciers terminate as massive tidewater glaciers.

[8] Farther north, the South Shetland Islands experience a transitional climate between subpolar and temperate, with winter temperatures between −3 and −5°C and summer temperatures above freezing [*Reynolds*, 1981; *King et al*., 2003]. Over the past four decades, this area has warmed 3.7 ± 2.1°C per century, the second fastest warming documented for Antarctica [*Vaughan et al*., 2003]. Approximately 170 mm of the total annual precipitation (~1200 mm) falls as rain during the summer months and produces more meltwater than along the WAP [*Yoon et al*., 1998; *Turner et al*., 2002]. Currently, the South Shetland Islands are covered in ice fields with a mean thickness of ~250 m that terminate both on land and in the sea [*Rückamp and Blindow*, 2011].

[9] Along the coastline of southern Chile, strong westerly winds generate a large precipitation gradient. Precipitation peaks at ~7000 mm yr^{-1} in the core of the westerlies, near 50°S, and decreases northward to ~2500 mm yr^{-1} at 40°S, and southward to ~500 mm yr^{-1} at 55°S [*Hulton et al*., 2002].

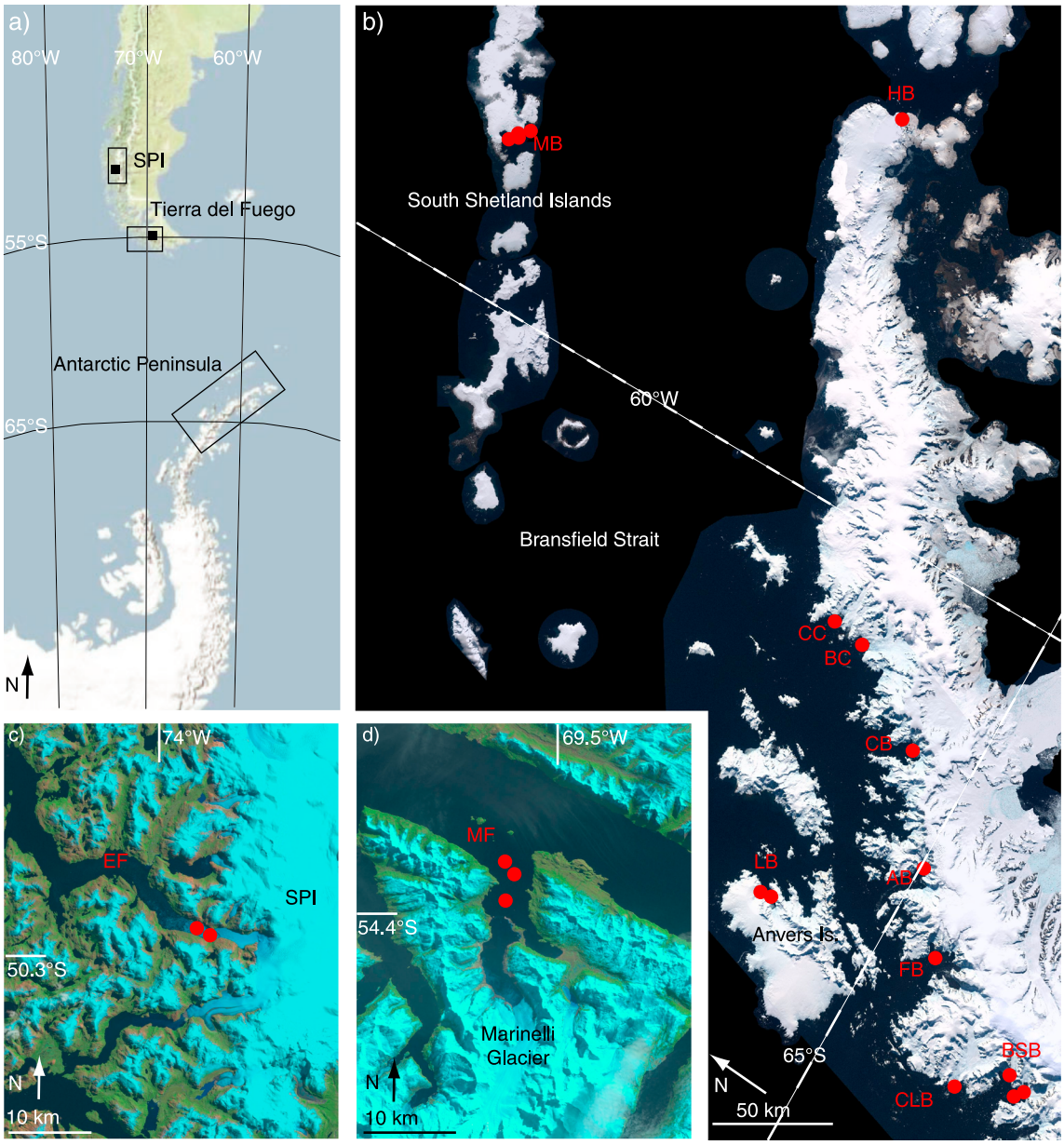

Figure 1. (a) Locations of the study areas outlined in black boxes. Expansion of the study sites in (b) the western Antarctic Peninsula, (c) Southern Patagonia ice field (SPI), and (d) Tierra del Fuego. Red circles represent core locations along the western Antarctic Peninsula in Figure 1b (NSIDC image), in Europa Fjord adjacent to the Southern Patagonia Icefield (SPI) in Figure 1c, and in Marinelli Fjord, Tierra del Fuego, in Figure 1d (USGS landsat images). All site names are abbreviated as in Table 1.

The northernmost study area reported herein, which is on the west side of the Southern Patagonia ice field, Europa Fjord (50°S), experiences ~4000 mm yr^{-1} of precipitation and a mean annual temperature of 7°C [*Hulton et al.*, 2002]. The second site in South America, Marinelli Fjord in Tierra del Fuego (54°S), typically receives between 500 and 1000 mm yr^{-1} of precipitation and annual temperatures average 5°C [*Hulton et al.*, 2002; *Boyd et al.*, 2008]. All of the glaciers entering the fjords of western Chile are temperate [*Anderson and Domack*, 1991].

3. ^{210}Pb Geochronology

[10] ^{210}Pb geochronology has been used to calculate recent sediment accumulation rates in a wide range of marine sedimentary environments [e.g., *Nittrouer et al.*, 1979; *Harden et al.*, 1992; *Dukat and Kuehl*, 1995; *Domack and McClennen*, 1996; *Jaeger et al.*, 1998; *Sommerfield and Nittrouer*, 1999; *Degeest et al.*, 2008]. Despite the considerable extent of coastlines in high latitudes and the amplified impacts of recent climate change in this region [*Holland and Bitz*, 2003; *Vaughan et al.*, 2003], few measurements of modern sediment accumulation exist along glaciated margins relative to their fluvial counterparts. ^{210}Pb forms naturally as one of the last daughter isotopes in the ^{238}U decay series and enters the marine environment in surface runoff and atmospheric precipitation; the in situ decay of its parent, ^{226}Ra, directly supplies ^{210}Pb to seawater. ^{210}Pb rapidly and irreversibly adsorbs to fine-grained particles

in suspension and is typically scavenged from the water column within a year in coastal waters [*Nittrouer et al*., 1979, and references therein]. Once deposited on the seabed, the adsorbed ^{210}Pb decays to its daughter ^{210}Bi with a half-life of 22.3 years until it reaches the activity supported by in situ decay of ^{226}Ra. The decay of excess ^{210}Pb, the activity of ^{210}Pb in excess of the supported level, can be used to study sediment accumulation over approximately a century.

[11] The sediment accumulation rate is calculated from the slope of the regression line fit to the semilog profile of excess ^{210}Pb activity versus depth. A typical decay profile contains three distinct zones with depth in the seabed: a surface layer, a region of logarithmic decrease, and a zone of supported activity. The upper portion of the profile often contains a surface layer (~10 cm thick) of uniform activity due to physical and biological particle mixing, above a zone of log linear decrease [*Nittrouer et al*., 1979]. This decrease represents steady state accumulation, assuming the activity of newly supplied sediment remains constant (Figure 2a; a comprehensive review of ^{210}Pb sediment-dating models is presented in *Appleby* [2002]). If the accumulation rate changes and stabilizes at a different rate, the log linear profile shows two linear sections with a break in slope (Figure 2c) [e.g., *Bentley et al*., 1996; *Sommerfield and Nittrouer*, 1999; *Palinkas and Nittrouer*, 2006]. Where the substrate is physically quiescent and subsurface burrowers are uncommon, ^{210}Pb profiles can show steady state accumulation (i.e., log linear decay) extending from the sediment surface [e.g., *DeMaster et al*., 1985]. The third distinct zone occurs below the region of linear decrease and is characterized by nearly uniform ^{210}Pb activity supported by the decay of its effective parent, ^{226}Ra, in the seabed.

[12] If accumulation rates have varied in time, the vertical profile of excess ^{210}Pb can still reveal temporal information about sediments reaching the seabed. If either the ^{210}Pb activity of the newly supplied sediment or the accumulation rate change on short time scales ($<$10 years), the profile will show fluctuating activity with no clear vertical pattern (Figure 2d) [e.g., *Dukat and Kuehl*, 1995; *Jaeger and Nittrouer*, 1999]. Episodic sediment delivery events, such as submarine gravity flows, create distinct zones in ^{210}Pb profiles that typically consist of low excess activity due to the high concentration of particles that settle on the seabed and compete for limited ^{210}Pb [e.g., *Mullenbach and Nittrouer*, 2000]. Low-activity regions can also reflect deposition of coarse-grained particles, as their surface area is relatively small and adsorbs less ^{210}Pb (Figure 2b) [e.g., *Nittrouer et al*., 1979; *Kuehl et al*., 1989]. The specific ^{210}Pb activity of particles depends on many oceanographic factors, including (1) circulation patterns in the fjords and shelf, (2) the depth of water through which the particle settles, and (3) ^{210}Pb concentration of fjord waters.

4. Methods

[13] Two cruises in 2005 and 2007 aboard the RV/IB *Nathaniel B. Palmer* provided the sediment core and bathymetric data presented here. The first cruise, NBP0505, collected the five kasten cores used in this study from two fjords in southern Chile spanning 50°S to 54°S (Figures 1c and 1d). An additional 16 kasten cores were collected from 10 bays and fjords in the South Shetland Islands and along the WAP during the 2007 cruise, NBP0703 (Figure 1b). Prior work had shown that the distribution of sediments is highly variable in Antarctic Peninsula fjords and bays [*Griffith and Anderson*, 1989]; thus, our initial survey collected multibeam maps and 3.5 kHz Compressed High Intensity Radar Pulse (CHIRP) seismic surveys to identify locations where sediments are ponded in glacier proximal settings. Sediment coring was guided by results from these surveys. In several of the fjords, ice distal cores were also collected to examine variations in sedimentation along a fjord axis.

[14] Onboard the RV/IB *Palmer*, the 3 m long kasten cores were photographed, described, and subsampled for further analysis. The top 25–50 cm was sampled in 1 cm increments for ^{210}Pb dating; the underlying sediments were sampled every 2 cm to an approximate depth of 1 m, followed by sampling every 5 cm to a depth of 2 m. If the core was longer than 2 m, samples were obtained every 10 cm in the lowermost section. The samples were placed in sterile bags and refrigerated until they were analyzed in the laboratory. Archive sections of each core were sent to the Antarctic Marine Geology Research Facility at Florida State University, where X-radiographs of the half-round subcores were obtained (note that images are shown as X-radiograph positives, where lighter colors indicate relatively fine grained sediment).

[15] Sediment accumulation rates were calculated by generating profiles of excess ^{210}Pb using a procedure similar to *Nittrouer et al*. [1979]. Sediment samples were homogenized, dried at 70°C, and crushed. The dry bulk density (indicated as "bulk density" hereafter) for each sample was calculated by comparing the wet and dry sediment weights, assuming a particle density of quartz (2.65 g cm^{-3}). A known activity of ^{209}Po was added to approximately 5 g of each sample. The sediment was then digested with solutions of both 15.8 N HNO_3 and 6 N HCl, and the Po isotopes were plated onto a silver planchet for ~20 h. Alpha spectroscopy was used to measure the activity of ^{209}Po and ^{210}Po, and the total ^{210}Pb activity in each sample was calculated based on measured values of ^{210}Po, the granddaughter isotope. Excess ^{210}Pb values were calculated by subtracting the supported activity at depth in the core from the total activity measured. A mean supported activity level of 0.9 ± 0.2 dpm g^{-1} was determined from the region of low, uniform activity below the zone of logarithmic decay. This value was observed in profiles from both the Chilean and WAP study sites that had steady state accumulation and was used to calculate excess activities for all cores.

[16] Sediment accumulation rates (mm yr^{-1}) were determined using least squares linear regression of the semilog profile. Mass accumulation rates (g cm^{-2} yr^{-1}) were calculated using the mean bulk density from each core. For profiles with a distinct, visual change in slope within the log linear region, linear regression was applied to each line segment, providing two accumulation rates. Profiles with r^2 values <0.75 were considered nonsteady state and classified as either vertically uniform or varying, depending on the pattern of ^{210}Pb activity with depth (see Table 1). For cores whose ^{210}Pb profiles suggested nonsteady accumulation with depth, detailed grain-size distributions were generated on specific intervals using a Malvern laser particle diffractor [*McCave et al*., 1986].

5. Results

[17] For each core site, the sediment accumulation rate and other pertinent information are compiled in Table 1. Additional context for each core site follows.

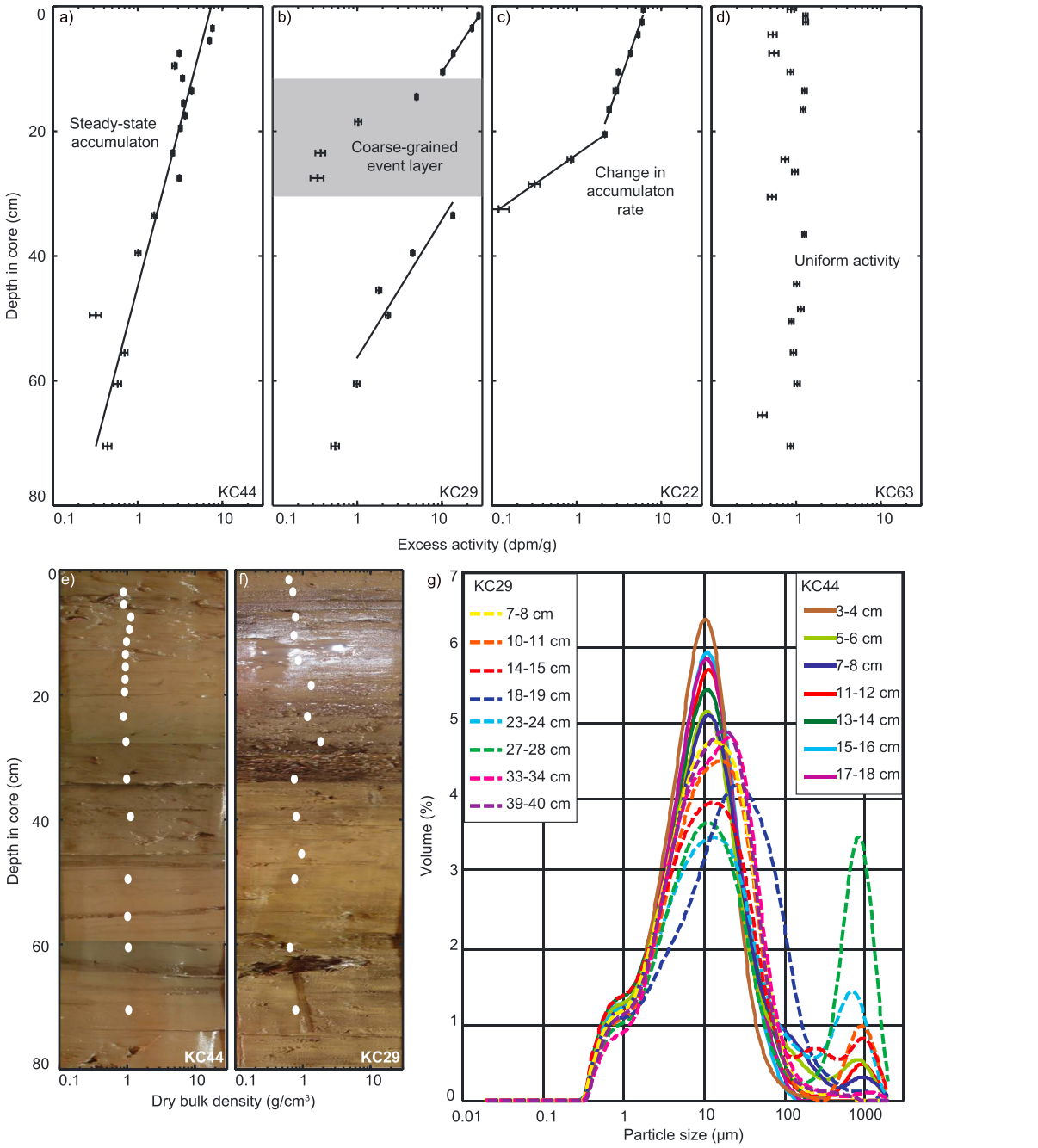

Figure 2. Four types of ^{210}Pb profiles were observed in this study: (a) steady state accumulation, (b) an event layer indicated by a region of lower ^{210}Pb activities in an otherwise steady state profile, (c) a change in the rate of steady state accumulation, and (d) complex accumulation or grain-size characteristics with slight variability in activity with depth in the core. (e and f) Representative core photographs and associated profiles of bulk density (white circles): one reflecting steady state accumulation (KC44) and a second steady state core with an event layer (KC29). (g) Intervals with elevated bulk densities in KC29 are those with relatively coarse grained sediments and bimodal grain-size distributions.

5.1. Western Antarctic Peninsula

[18] The four southernmost samples in this study were collected from the Graham Coast: three cores from Beascochea Bay (BSB), KC44, 45, and 48, and core KC41, from Collins Bay (CB) (Figures 1b, 3a, and 3b). Cores KC44 and KC45, collected in a deep trough just seaward of Cadman Glacier (Figure 3a), contain relatively uniform profiles of bulk density and steady ^{210}Pb accumulation at rates of 7.0 and 2.2 mm yr^{-1}, respectively ($r^2 = 0.83$, 0.96; Figures 3c and 3d). KC48, in front of the Lever Glacier (Figure 3a), shows a steady state accumulation profile of 6.4 mm yr^{-1}, overlain by ~40 cm of sediment with lower bulk density and relatively uniform, excess ^{210}Pb activity that decreases slightly in the uppermost 5 cm (Figure 3e). The entire length of KC41 contains generally uniform bulk density

Table 1. Core Information Summary

Core	Location[a]	Latitude (°S)	Longitude (°W)	Core Length (m)	Accumulation Rate (mm yr^{-1})	Accumulation Style[b]	Distance From Ice Front (km)
			Southern Chile				
KC28P	Europa Fjord (EF)	50.278	73.949	2.0	N/D[c]	varying	7.1
KC35P	Europa Fjord	50.282	73.923	2.0	11.4	SS	5.2
KC50P	Marinelli Fjord (MF)	54.390	69.591	1.2	23.6	SS	12.3
KC79P	Marinelli Fjord	54.350	69.585	1.1	N/D	varying	17.1
KC80P	Marinelli Fjord	54.361	69.577	2.0	N/D	varying	16.6
			South Shetland Islands				
KC14	Maxwell Bay (MB)	62.196	58.833	1.6	5.5, 2.0[d]	change in SS	3.4
KC21	Maxwell Bay	62.205	58.739	0.45	6.6, 2.8	change in SS	0.2
KC22	Maxwell Bay	62.214	58.777	2.17	5.2, 1.3	change in SS	1.9
KC23	Maxwell Bay	62.253	58.710	0.39	1.6, 1.4	SS, event	4.8
			Antarctic Peninsula				
KC10	Hope Bay (HB)	63.386	57.010	0.34	3.0	SS	3.5
KC65	Cierva Cove (CC)	64.157	60.863	0.48	N/D	vertically uniform	1.0
KC63	Brailmont Cove (BC)	64.290	60.982	1.2	N/D	vertically uniform	0.1
KC33	Lapeyrere Bay (LB)	64.373	63.289	2.9	2.2	SS	1.2
KC28	Lapeyrere Bay	64.402	63.252	2.9	3.2	SS	6.8
KC60	Charlotte Bay (CB)	64.632	61.519	0.36	2.8	SS	3.2
KC57	Andvord Bay (AB)	64.872	62.425	1.3	5.6	SS, event	0.8
KC29	Flandres Bay (FB)	65.066	63.103	1.9	2.8, 3.0	SS, event	5.7
KC41	Collins Bay (CLB)	65.346	63.056	2.7	N/D	vertically uniform	1.2
KC48	Beascochea Bay (BSB)	65.510	63.708	1.0	6.4	SS, event	0.9
KC45	Beascochea Bay	65.589	63.830	1.0	2.2	SS	2.0
KC44	Beascochea Bay	65.607	63.817	1.8	7.0	SS	0.7

[a]The location acronym in parentheses refers to core sites shown in Figure 1.

[b]Accumulation styles include steady state (SS; Figure 2a), varying ^{210}Pb activity with depth, SS with an event layer (Figure 2b), change in SS rate (Figure 2c), and relatively uniform ^{210}Pb activity with depth (all excess or all supported; Figure 2d).

[c]Accumulation rates for nonsteady core types cannot be determined (N/D).

[d]The first rate refers to the more recent sediments.

and varying excess ^{210}Pb activity of 0.6–1.4 dpm g^{-1}, nearly all of which falls within the 0.9 ± 0.2 dpm g^{-1} range of supported activity for this region (Figure 3f). X-radiographs of regions showing steady accumulation are characterized by relatively homogenous sediment with some dropstones and few, faint laminations (Figures 3g–3j). In the upper section of KC48 with high, uniform ^{210}Pb activities, the X-radiograph reveals millimeter-scale laminations (Figure 3i), while X-rays of KC41 show relatively homogeneous sediment with few visible laminations (Figure 3k). Of the cores collected along the WAP, KC44 and KC48 were collected near the ice front for two of the largest WAP glaciers; they record the fastest sediment accumulation for this region (Table 1).

[19] Slightly farther to the north, in Flandres Bay (FB; Figures 1b and 4a), core KC29 shows steady state accumulation separated by a 10 cm thick section characterized by much lower ^{210}Pb activity (Figure 4d). Below this low-activity layer, sediment accumulated at 3.0 mm yr^{-1}, and above the layer, modern sediment has accumulated at 2.8 mm yr^{-1} ($r^2 = 0.90$, 0.99; Figure 4d). The X-radiograph image and grain-size analyses of the particles in the low-activity region indicate this section is coarser (darker color in X-ray, mean size of 1.0 mm versus 0.01 mm) and is denser than the rest of the deposit. Likely, the coarse grain size (reduced surface area) accounts for both the decrease in ^{210}Pb activity and increases in density (Figures 2f, 2g, and 3d). Along the Danco Coast, core KC57 from Andvord Bay (AB; Figure 4b) contains a region of uniform bulk density and steady state ^{210}Pb accumulation at 5.6 mm yr^{-1} ($r^2 = 0.97$) overlain by a 60 cm thick deposit containing varying bulk density and ^{210}Pb activity (Figure 4e). ^{210}Pb from core KC60 in Charlotte Bay (CB; Figure 4c) shows bulk density increasing slightly with depth and steady sediment accumulation at a rate of 2.8 mm yr^{-1} ($r^2 = 0.93$) (Figures 1b and 4f). X-radiographs of steady state ^{210}Pb regions reveal fine-grained deposits with scattered small dropstones and faint laminations (Figures 4g, 4i, and 4j), whereas images from nonsteady regions show coarser-grained (darker) intervals and more distinct layering (Figures 4g and 4h).

[20] On Anvers Island, nearly 3 m long cores were collected in each of the two arms of Lapeyrere Bay (LB; Figures 1b and 5a). KC33 and KC28 both show uniform bulk density with depth and steady state ^{210}Pb accumulation; rates are 2.2 mm yr^{-1} ($r^2 = 0.96$) and 3.2 mm yr^{-1} ($r^2 = 0.98$), respectively (Figures 5b and 5c). X-radiographs from both cores show fine-grained sediment with small dropstones throughout (Figures 5d and 5e). Sediment accumulates faster at the more ice distal site, and seismic profiles from the main fjord basin (where KC28 was collected) show the thickest sediments, reflecting greater input from Illiad Glacier, the largest glacier entering the basin [*Griffith and Anderson*, 1989, Figure 12].

[21] Proceeding north, one core was collected each in Cierva and Brailmont Coves off Hughes Bay (BC and CC; Figures 1b and 6a). Excess ^{210}Pb activity in core KC63 from Brailmont Cove is relatively uniform and low within 90 cm of the seabed (Figure 6c). KC65 from Cierva Cove contains uniform excess ^{210}Pb activity that extends from the surface to a depth of 36 cm (Figure 6b). In both cores, bulk density fluctuates with depth. The X-radiograph from KC65 shows very few laminations and some dropstones, while the image from KC63 shows millimeter to centimeter scale laminations throughout the core (Figures 6d–6f). The northernmost core on the WAP, KC10, from the center of Hope Bay (HB; Figures 1b and 7a), contains sediment with bulk densities that

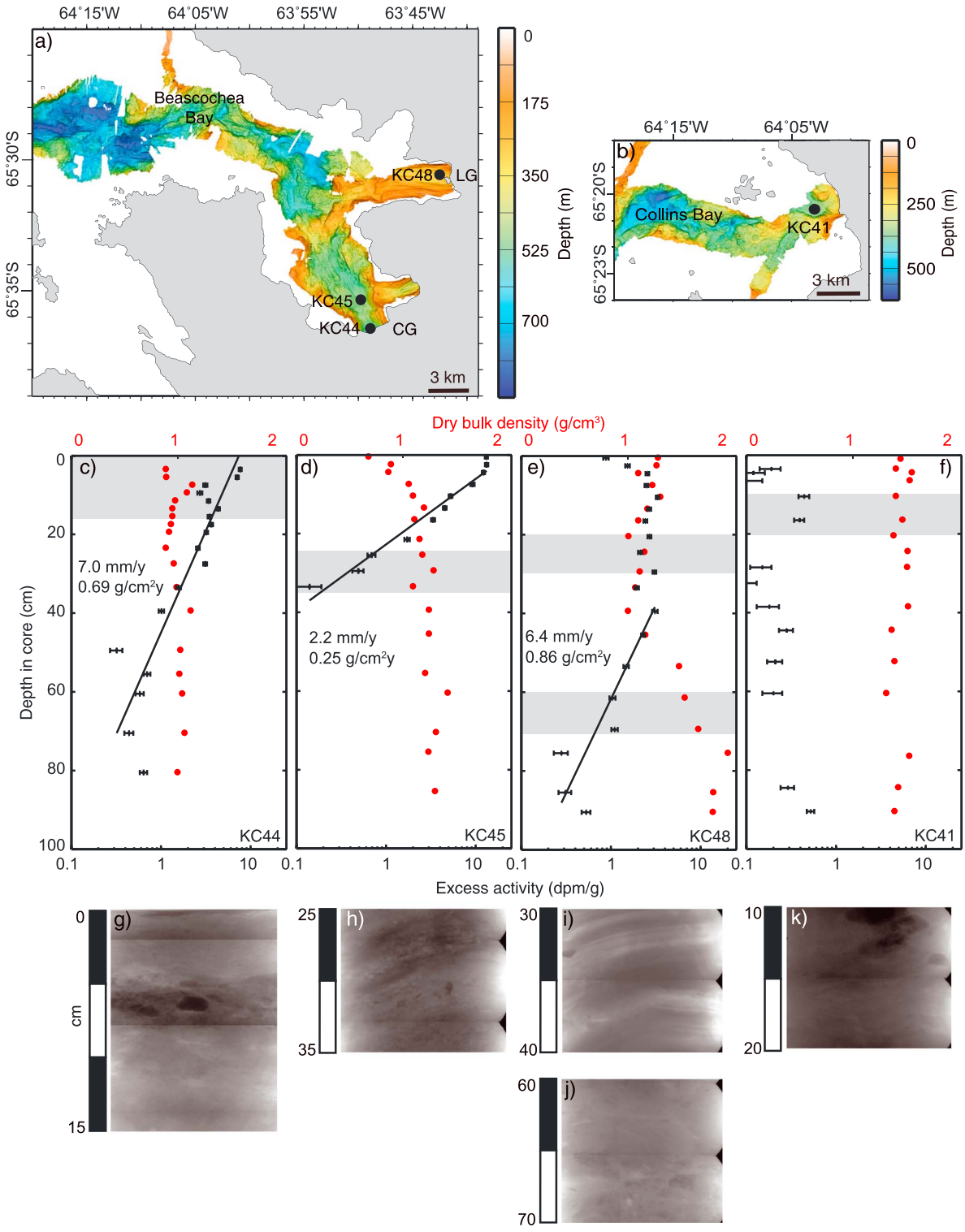

Figure 3. (a, b) Bathymetry for Beascochea and Collins Bays, with locations of the four ice proximal cores. LG and CG show locations of Lever Glacier and Cadman Glacier, respectively. Land and glacier-covered areas are shown in light gray; marine regions beyond the multibeam bathymetric data are colored white. (c, d) Cores KC45 and KC44 show steady state ^{210}Pb accumulation (black symbols; lower abscissa), with relatively uniform bulk density profiles (red dots, upper abscissa). (e) KC48 records steady state accumulation in front of Lever Glacier below a region of relatively uniform, high excess activities and lower bulk densities. (f) KC41 from Collins Bay shows uniform, low excess ^{210}Pb activities, corresponding to relatively uniform bulk densities. (g–k) Representative positive X-radiographs below each core image the gray-shaded areas in the profiles (note artifacts of X-radiograph processing: black triangles along the right edge and corresponding dark horizontal lines).

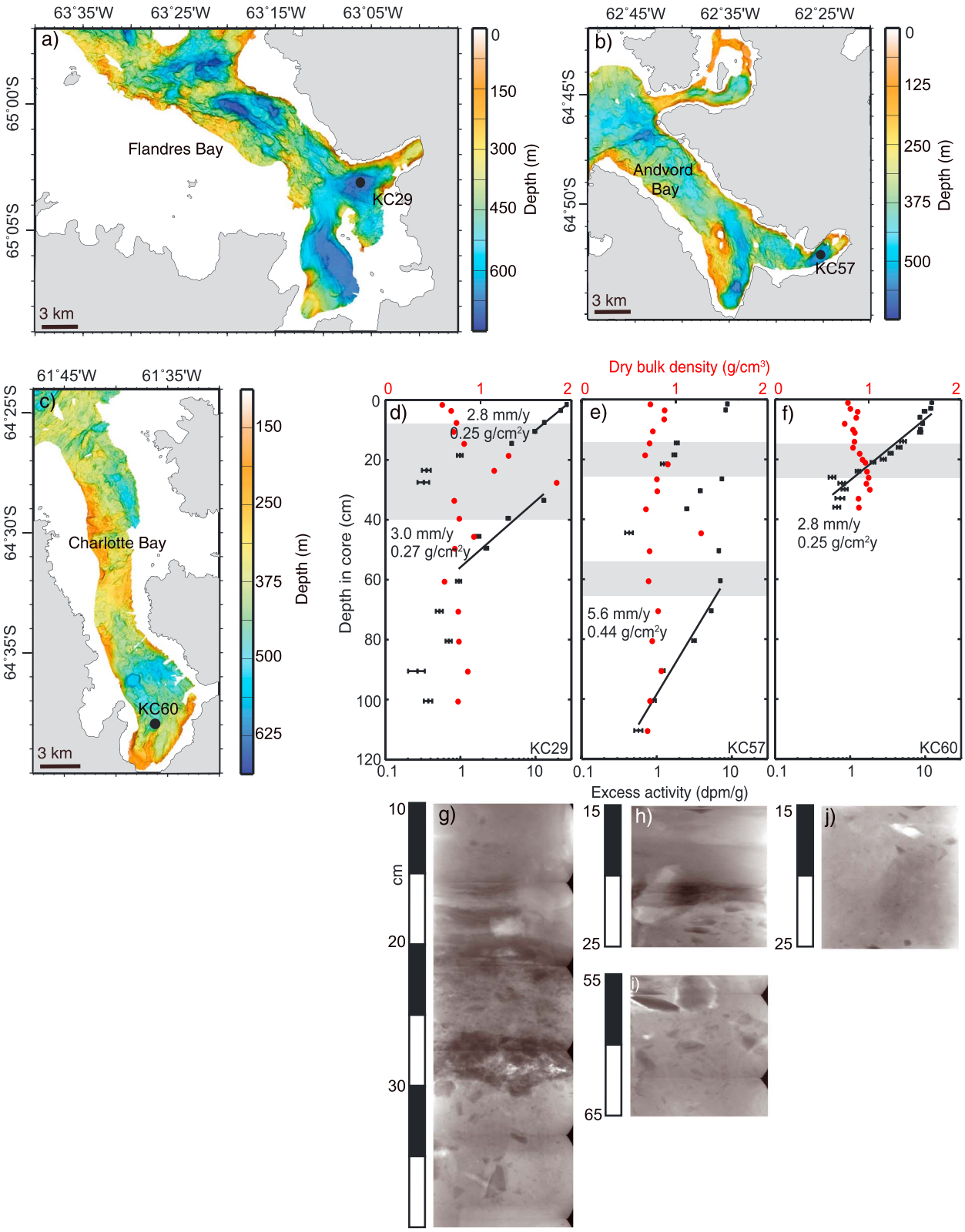

Figure 4. (a–c) Land and glacier area (light gray), and multibeam bathymetry for Flandres, Andvord, and Charlotte Bays, with core locations indicated. Symbols are the same as for Figure 3. (d) A section of relatively low excess activity and higher bulk density interrupts otherwise steady accumulation in KC29, (e) steady state sediment accumulation with uniform bulk density in KC57 was followed by accumulation with varying ^{210}Pb activity and density, and (f) relatively uniform bulk densities and steady state accumulation of 2.8 mm yr^{-1} characterize KC60. (g–j) X-radiograph positives are shown for core sections shaded in gray and reveal stratification and numerous dropstones.

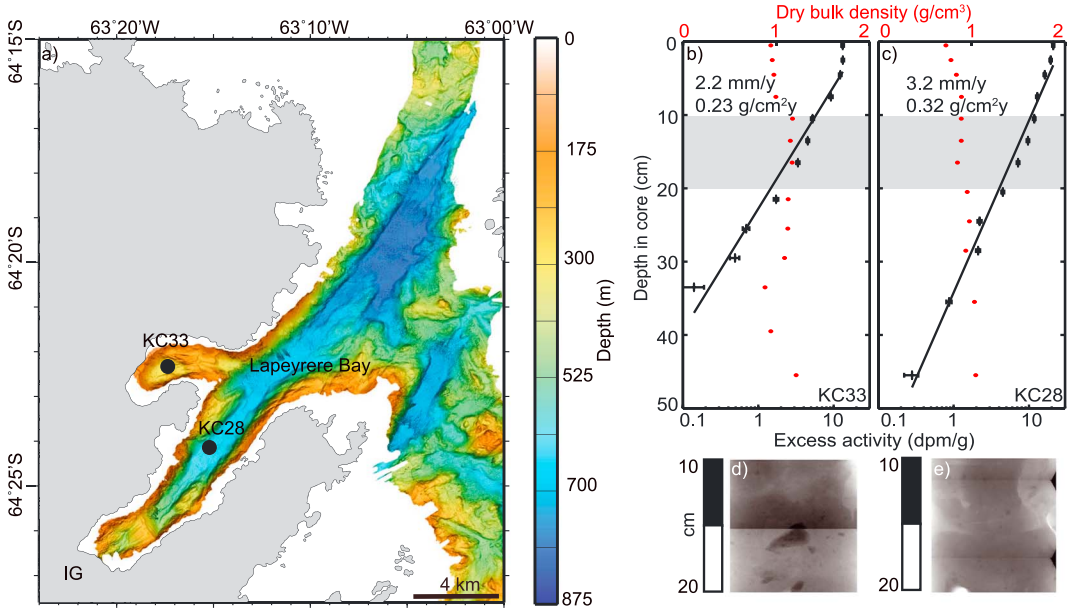

Figure 5. (a) Core locations from Lapeyrere Bay shown with multibeam bathymetry. IG indicates the location of Illiad Glacier. (b, c) Profiles of excess ^{210}Pb and bulk density indicate steady state accumulation in KC33 and KC28. (d, e) X-radiograph positives highlight shaded intervals in KC33 and KC28. Dark triangles and horizontal lines are artifacts of X-radiograph processing. Colors and symbols are explained in Figure 3.

slightly increase with depth and steady ^{210}Pb accumulation at 3.0 mm yr^{-1} ($r^2 = 0.95$; Figure 7b). X-radiographs reveal homogenous sediment with no evidence for layering (Figures 7c and 7d).

5.2. South Shetland Islands

[22] Four sediment cores were collected in three coves that fringe Maxwell Bay (MB) on King George Island (Figures 1b and 8a). ^{210}Pb profiles for three of these cores

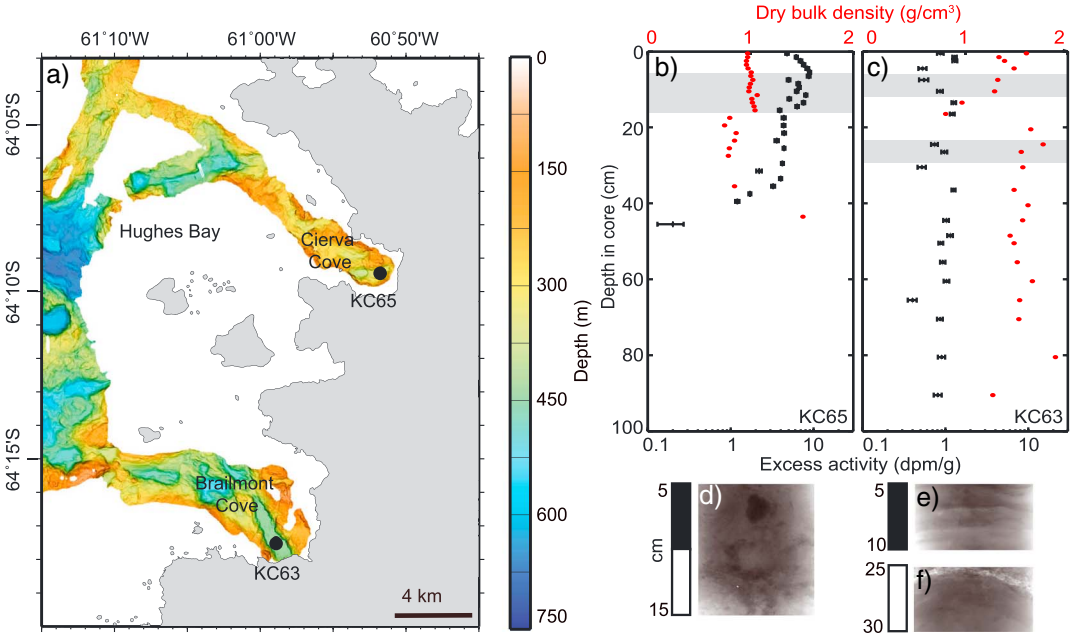

Figure 6. (a) Core locations in ice proximal depocenters and multibeam bathymetry for Hughes Bay. Both the excess ^{210}Pb profiles for (b) KC65 from Cierva Cove and (c) KC63 from Brailmont Cove show relatively uniform high and low excess activities, respectively, extending the length of the cores. Bulk density profiles indicate fluctuations downcore, consistent with those in ^{210}Pb activity. (d–f) X-radiograph positives corresponding to gray-shaded areas show scattered dropstones and laminations. Colors and symbols are explained in Figure 3.

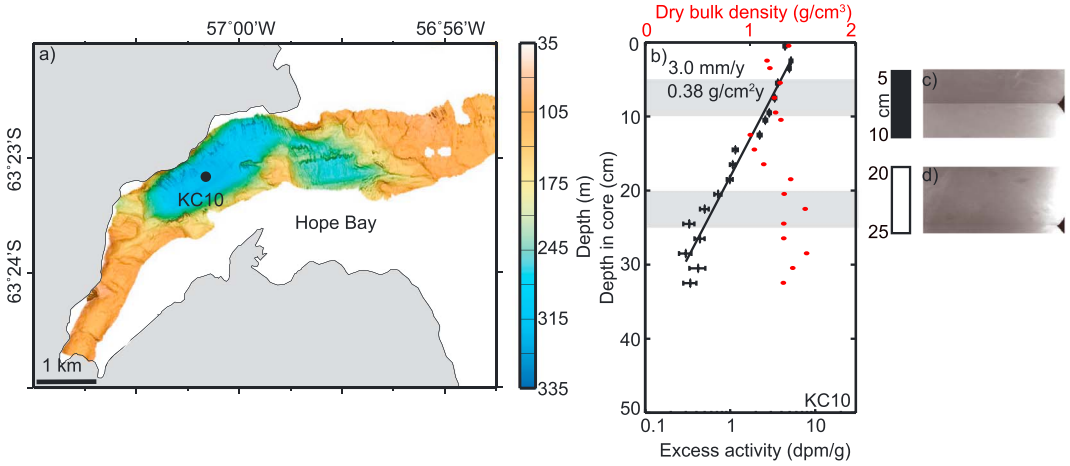

Figure 7. (a) Multibeam bathymetry and core location for Hope Bay. (b) The excess ^{210}Pb profile for core KC10 indicates steady state accumulation; bulk densities fluctuate from ~1 to 1.7 g cm^{-3}. (c, d) The X-radiograph images highlight the gray-shaded regions in Figure 7b. Dark triangles and horizontal lines are artifacts of X-radiograph processing. Colors and symbols are explained in Figure 3.

show a distinct change in the rate of accumulation, in all cases increasing by a factor of 2 to 4 in the last few decades (Figures 8b–8d). The accumulation rate determined for KC14 in the inner bay increased from 2.0 to 5.5 mm yr^{-1} around 1980 (respective $r^2 = 0.98$; Figure 8b). In core KC21, from Marion Cove, the rate increased from 2.8 to 6.6 mm yr^{-1} around 1984 ($r^2 = 0.99$, 0.91; Figure 8c). Similarly for KC22, also collected in Marion Cove slightly farther from the current glacier terminus, the rate increased from 1.3 to 5.2 mm yr^{-1} around 1978 ($r^2 = 1.0$, 0.97; Figure 8d). X-radiographs from the region of change in each of the ^{210}Pb profiles do not indicate a similar change in the sediment composition or structure; all cores contain ice-rafted debris and no apparent layering (Figures 8f–8h). KC23, near the mouth of Potter Cove, was the most seaward and ice distal core collected in Maxwell Bay. Unlike the other cores, KC23 contains an ~8 cm thick interval characterized by relatively uniform excess ^{210}Pb activity that punctuates the otherwise steady accumulation of ~1.5 mm yr^{-1} ($r^2 = 0.94$, 0.91; Figure 8e); however, a distinct change in the sediment composition or structure is not visible in the X-radiograph (Figure 8i). Bulk densities are relatively uniform in all cores, except in KC21, where they increase with depth. A statistical comparison shows no correlation between bulk density and ^{210}Pb activity.

5.3. Chilean Fjords

[23] In Tierra del Fuego, three cores were collected in the outer basin of Marinelli Fjord (MF; Figure 1d). Closest to the glacier, at KC50P, sediment has accumulated steadily at 23.6 mm yr^{-1} ($r^2 = 0.87$; Figure 9a), while ^{210}Pb profiles from cores KC79P and KC80P, both in the distal, outer region of the fjord, indicate variable low ^{210}Pb activities (Figures 9b and 9c). Our two northernmost cores were collected from the long, narrow Europa Fjord (EF; Figure 1c), on the southwest side of the Southern Patagonia ice field. The ^{210}Pb profile from KC28P, 7.1 km from the ice front, indicates varying and very low ^{210}Pb activities (Figure 9d), whereas KC35P, 5.2 km from the ice front, records steady state accumulation at 11.4 mm yr^{-1} ($r^2 = 0.83$; Figure 9e). In all five cores, bulk density is uniform with depth around 1 g cm^{-3}, with the exception of the basal portion of KC80P, where the density is greater. Only the X-radiograph from KC79P indicates distinct centimeter-scale layering; X-radiographs of the other cores show homogenous sediment (Figures 9f–9j).

6. Discussion

6.1. Interpretation of ^{210}Pb Profiles

6.1.1. Steady Accumulation Rates

[24] In 15 of the 21 cores presented here, profiles of excess ^{210}Pb indicate that sediments have been accumulating at a relatively constant rate over approximately the last century, suggesting that the frequency, magnitude, and source of sediment delivery events have not changed appreciably in time (Figures 3c, 3d, 4f, 5b, 5c, 7b, 8b–8d, 9a, and 9e). X-radiographs of these cores all show deposits with little visible layering and a uniform scattering of ice-rafted debris, consistent with steady sediment accumulation at rates of a few mm yr^{-1} (Figures 3g–3j, 4j, 5d, 5e, 7c, 7d, and 8f–8h). Previous studies have observed similar steady state ^{210}Pb profiles in WAP fjords and in basins relatively distant from glaciers [e.g., *Harden et al.*, 1992; *Domack and McClennen*, 1996]. Such steady state sediment accumulation at the stationary core sites throughout the last century is surprising in view of the extreme environmental changes that have occurred during this period. The increase in mean annual temperatures along the WAP measured over the last 50+ years exceeds the global average sixfold [*Vaughan et al.*, 2003]. This exceptional warming, together with the coincident increase in melt percentage to a level unprecedented during the last millennium [*Abram et al.*, 2013], would likely accelerate glacial sliding, erosion, and sediment transport to fjords. But this expected increase in sediment accumulation at any site would tend to be offset by the substantial recent glacial retreat in this region: Over 87% of the glaciers in the Peninsula have retreated (mean ~580 m, max ~5 km) in the past 50+ years [*Cook et al.*, 2005; *Pritchard and Vaughan*, 2007]. Because rates of accumulation generally decrease exponentially down fjord [e.g., *Cowan*

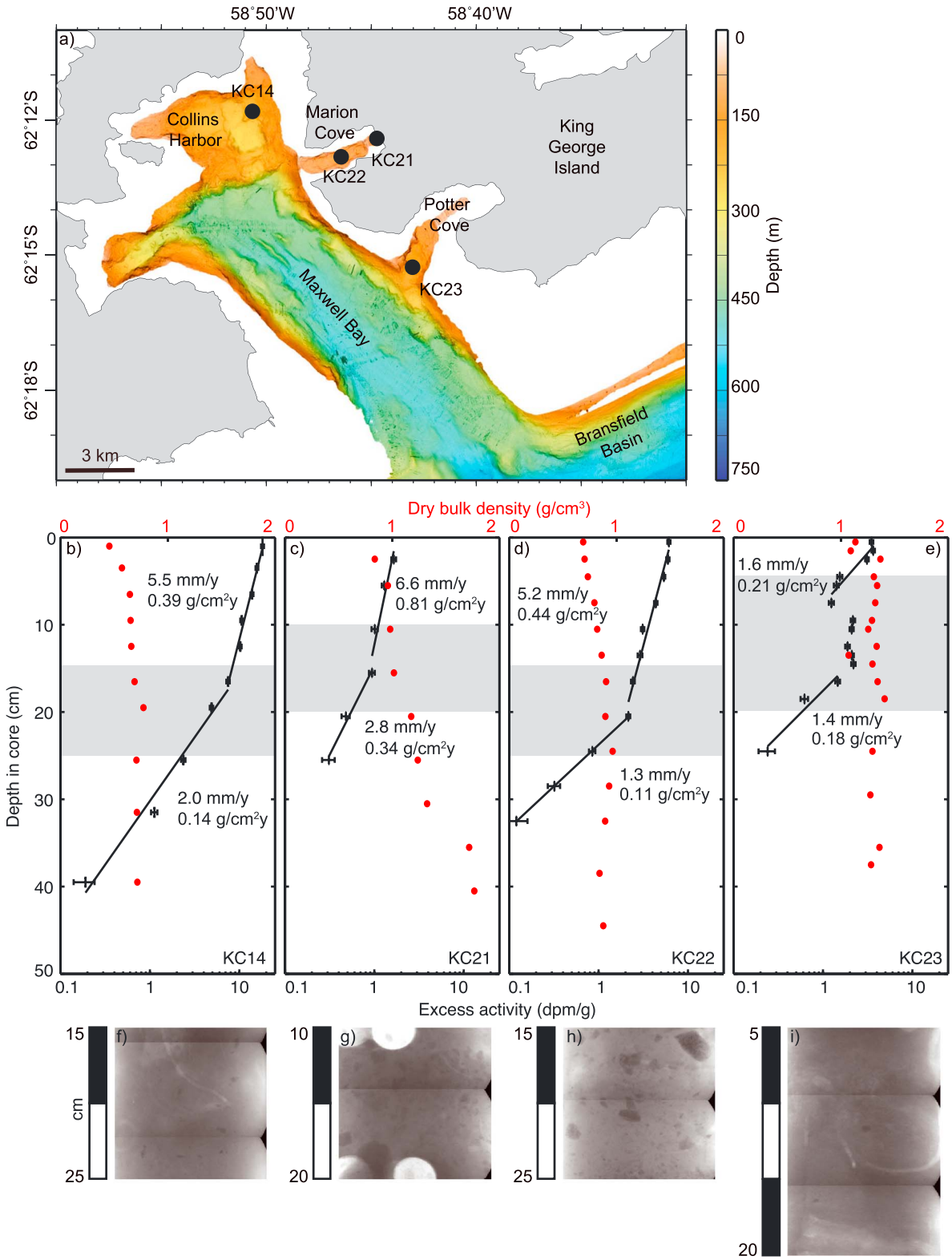

Figure 8. (a) Multibeam bathymetry and core locations near Maxwell Bay, South Shetland Islands. (b–d) ^{210}Pb profiles for the three ice proximal cores; distinct break in slopes reflects abrupt increase in accumulation rate. (e) KC23, the most ice distal, contains an event layer between the regions of steady state accumulation. Bulk densities are relatively uniform in all cores except KC21, where they increase with depth. (f–i) X-radiograph images correspond to the areas shaded in Figures 8b–8e, with numerous dropstones visible in Figures 8g and 8h. Dark horizontal lines extending from black triangles along the right edge of each image are artifacts of X-radiograph processing. White circles in Figure 8g are empty spaces where samples were collected. Colors and symbols are explained in Figure 3.

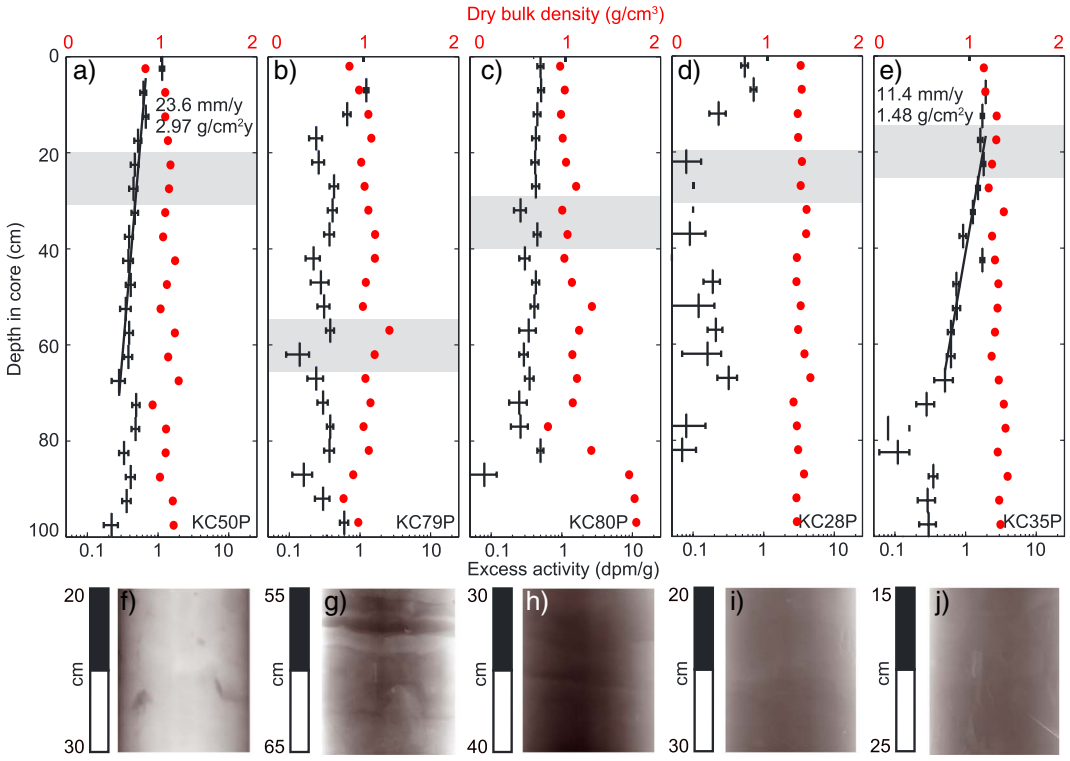

Figure 9. Five cores collected from southern Chile. Marinelli core (a) KC50P records the fastest steady accumulation in this study, 23.6 mm yr^{-1}. (b) KC79P and (c) KC80P from the outer Marinelli Fjord contain ^{210}Pb profiles with varying activity. (d) KC28P and (e) KC35P from Europa Fjord show varying, low activity and steady state accumulation, respectively. The bulk density is relatively uniform and close to 1 g cm^{-3} for all cores except for the base of KC80P. (f–j) X-radiograph positives show the regions shaded in gray. Symbols are explained in Figure 3.

et al., 1997; *Jaeger and Nittrouer*, 1999], and glacial retreat increases the distance between the ice front and any proglacial core site, accumulation rates would tend to decrease with time at any core site, thereby tending to offset the increase in sediment yields expected due to the warming climate.

6.1.2. Changes in Accumulation Rate

[25] In contrast with the steady state profiles of excess ^{210}Pb collected from the WAP, profiles in the South Shetland Islands appear consistent with ongoing climatic changes in this region, which experiences a relatively warm and wet climate. Three of the four ^{210}Pb profiles show a break in slope (Figures 2b and 8b–8d), reflecting a recent two-to-fourfold acceleration of accumulation for the three ice proximal cores, which agrees well with independent analyses of other Maxwell Bay cores [*Yoon et al*., 2000, 2010; *Monien et al*., 2011; *Majewski et al*., 2012]. Although the X-radiographs show no visible change in the sedimentary character, the timing of the accumulation rate increase was ~25 years ago and coincides with the period during which glaciers north of 64°S retreated the fastest [*Cook et al*., 2005]. The increase in accumulation rate preserved in the sedimentary record may reflect a sensitive transition in the glaciers of the South Shetland Islands from subpolar to temperate. The increase in nearby surface temperatures and in the frequency of precipitation events, measured since ~1969 and ~1956, respectively [*Turner et al*., 1997; *Vaughan et al*., 2003], could increase sediment accumulation rates by generating more vigorous periglacial weathering and mass wasting, as well as increased volumes of meltwater, which transport sediment to Maxwell Bay [*DaSilva et al*., 1997; *Yoon et al*., 1998]. The trends observed in the ^{210}Pb profiles from Maxwell Bay suggest that if the region continues to warm, increased meltwater production and faster sediment accumulation could extend to the WAP.

6.1.3. Complex ^{210}Pb Profiles

[26] In addition to steady accumulation described above, some of the ^{210}Pb profiles exhibit a variety of sediment accumulation patterns and reflect diverse glacimarine sedimentary processes. Vertically uniform profiles with significant excess ^{210}Pb typically indicate rapid, possibly instantaneous, sediment deposition. The high activities (such as KC65; Figure 6b) suggest (1) a relatively vigorous circulation of seawater renews the inventory of ^{210}Pb in the local water column and/or (2) the sediments entered the fjord entrained in a buoyant surface plume from which they settled through deep water columns, scavenging ^{210}Pb. Vertically uniform profiles with low activities (KC41 and KC63; Figures 3f and 6c), however, could represent supported ^{210}Pb values (~0.9 dpm g^{-1}), and thus sediment sufficiently old (>100 years) for all excess ^{210}Pb to have decayed to negligible levels. Alternatively, these ^{210}Pb profiles could indicate the deposition of particles with negligible excess ^{210}Pb activity, which would occur if particles were delivered by gravity flows with mixtures of glacial meltwater and limited seawater [e.g., *Dukat and Kuehl*, 1995; *Mullenbach and Nittrouer*, 2000].

[27] Four of the profiles characterized by steady state accumulation are interrupted by ~10 to 60 cm thick zones of

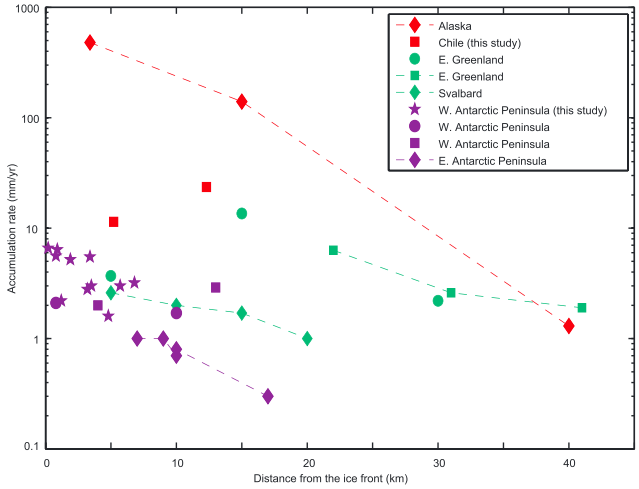

Figure 10. Compilation of published ^{210}Pb-derived accumulation rates for glacially influenced fjords. Temperate fjords in Alaska (red diamonds [*Cowan et al*., 1997]) and Chile (red squares, this study); subpolar fjords in east Greenland (green circles [*Smith et al*., 2002], green squares [*Andresen et al*., 2011]) and Svalbard (green diamonds [*Szczucinski et al*., 2009]); and cold subpolar to polar fjords in the Western Antarctic Peninsula (purple stars, this study; purple circles [*Domack and McClennen*, 1996]; purple squares [*Harden et al*., 1992]) and the Eastern Antarctic Peninsula (purple diamonds [*Gilbert and Domack*, 2003]). Lines connect measurements within individual fjords.

relatively uniform excess ^{210}Pb activity; they represent one or many discrete, rapid depositional events (Figures 3e, 4d, 4e, and 8e), which can result from diverse sedimentary processes. Rapid settling from a sediment-laden meltwater plume would create a deposit of uniform, high excess activity (potential examples: KC48 and KC23; Figures 3e and 8e), while the release of a large volume of coarse ice-rafted debris or a gravity flow would form sediment intervals of low activity (e.g., KC29; Figure 4d). X-radiographs from these deposits help determine the formative sedimentary processes; for example, the low activity layer in KC29 corresponds to a region of concentrated coarse-grained material (Figures 2f, 2g, and 4g). Confidently distinguishing between these possibilities, however, would require additional data, such as shorter-lived radioisotopes to measure processes occurring on event time scales (e.g., weeks to months) [e.g., *Jaeger and Nittrouer*, 1999], and detailed evaluation of the individual cores is beyond the scope of this paper.

6.1.4. Biological Factors

[28] As mentioned earlier, biological factors can alter the distribution of ^{210}Pb within the cores and impact the interpretation of sedimentary processes and accumulation rates from profiles of excess ^{210}Pb. Burrowing benthic organisms can mix the upper sediment, potentially creating a zone of uniform activity like we see in a few of the cores, which otherwise show steady state accumulation (Figure 5b). Regional measurements of bioturbation intensity along the WAP indicate that burrowing is confined to the upper 8 cm and that local benthic organisms primarily utilize surface organic material year round [*McClintic et al*., 2008]. The steady accumulation profiles presented here all show log linear decay down to at least 30 cm depth in core (e.g., Figures 3d and 5c), which would be very deep for biological community mixing and implies little or no vertical mixing [cf. *Nittrouer et al*., 1984; *Harden et al*., 1992]. Moreover, X-radiographs do not show evidence of tubes or burrows.

[29] In addition to biological mixing, the fraction of biologically produced sediment accumulating on the seabed is also of considerable interest, especially when using total sediment masses to develop terrigenous sediment budgets and infer glacial erosion rates [*Koppes and Hallet*, 2002, 2006, 2010; *Cowan et al*., 2010; *Koppes*, 2012]. The coastal and shelf waters of the WAP support a productive biological ecosystem, in which sea ice cover primarily controls productivity during the austral summer [e.g., *Ducklow et al*., 2007]. The relative contribution of biogenic particles within the seabed generally increases with primary productivity and decreases as the accumulation rate of terrigenous sediment increases. Thus, the biogenic component generally increases southward, and with increasing distance from the ice front, due to the general decrease in rates of terrigenous sediment accumulation [e.g., *Dunbar et al*., 1985; *Griffith and Anderson*, 1989; *Domack and Ishman*, 1993]. In the productive waters of the Ross Sea, biogenic silica accounts for 1–7% by weight of total sediment accumulation in most areas, with a maximum contribution of ~40% in the southwestern Ross Sea [*Ledford-Hoffman et al*., 1986]. Along the WAP, biogenic silica accounts for <5% of total sediment particles in a polar fjord south of our study sites [*Gilbert et al*., 2003], ~12–14% in the outer portion of Andvord Bay [*Domack and Ishman*, 1993] and ~6% since the Little Ice Age in Maxwell Bay [*Milliken et al*., 2009]. Offshore of Maxwell Bay, measurements from the Bransfield Strait indicate biogenic contribution of ~12% in deep basins [*DeMaster et al*., 1991]. Thus, in our glacier proximal study sites, biogenic silica is likely to be a minor (i.e., <10%) component of the sediments.

6.2. N-S Transect Trends

[30] Along our 15° S-N transect, modern rates of sediment accumulation in temperate fjords of southern Chile substantially exceed those in the subpolar fjords of the South Shetland Islands and WAP (Table 1 and Figure 10). In Chilean fjords, rates range from 11.4 to 23.6 mm yr^{-1} (n = 2, mean = 17.5 mm yr^{-1}), whereas along the WAP and South Shetland Islands, they range from 1.3 to 7.0 mm yr^{-1} (n = 14, mean = 4.2 mm yr^{-1}). Moreover, the WAP and South Shetland Islands accumulation rates are 2 to 3 orders of magnitude smaller than ice proximal rates derived from seismic data in southern Chile, including Laguna San Rafael and Marinelli Fjord [*Koppes*, 2007; *Koppes et al*., 2009]. We suspect that this contrast is related to the abundance of meltwater in the Chilean glacier systems. The higher annual temperatures and precipitation in southern Chile favor meltwater production, which is likely to increase the basal water pressure leading to faster sliding [*Iken and Bindschadler*, 1986; *Anderson et al*., 2004; *Bartholomew et al*., 2010]. Additionally, high basal water pressures promote subglacial erosion by quarrying, especially where they fluctuate frequently [*Hallet*, 1996; *Iverson*, 2012]. Indeed, increases in sliding velocities (inferred from measured increases in the surface speed) have been correlated with increases in the production and transport of glacial sediment [e.g., *Humphrey and Raymond*, 1994; *Anderson et al*., 2004; *Riihimaki et al*., 2005].

[31] For the relatively cool and dry climatic regime in the southern part of this study, sediment accumulation rates in the South Shetland Islands and along the WAP do not decrease with increasing latitude as we had expected based upon previous studies [*Harden et al*., 1992; *Domack and McClennen*, 1996]. The transitional climate of the South Shetland Islands, plus the well-documented occurrence of seasonal debris-laden meltwater emanating from the King George Island ice cap [*Griffith and Anderson*, 1989; *Domack and Ishman*, 1993; *Yoon et al*., 1998], suggest that sediment accumulation rates should be intermediate between polar and temperate. The modern accumulation rates measured in Maxwell Bay, however, are just above the 4 mm yr^{-1} mean accumulation rate from the WAP and agree well with previous measurements [e.g., *Yoon et al*., 2000, 2010; *Majewski et al*., 2012]. These modest rates likely reflect the limited size and vigor of the glaciers and ice caps that cover the South Shetland Islands, compared to the ice masses along the WAP [*Koppes and Hallet*, 2010; *Koppes*, 2012].

[32] Within the WAP fjords, the accumulation rates of 3–7 mm yr^{-1} measured in this study are within the range of values reported previously [*Harden et al*., 1992; *Domack and McClennen*, 1996]. We stress that none of our sites represent a true polar setting, where basal meltwater would be negligible and glacial erosion rates would nearly vanish [*Cuffey et al*., 1999]. The lack of a distinct latitudinal pattern within these subpolar sites suggests that the expected general decrease in sediment accumulation rates with temperature is confounded by site-specific factors; these likely include the meltwater production regime, distance to the ice front, fjord bathymetry, the glaciated basin area, and ice flux [*Domack and McClennen*, 1996; *Koppes and Hallet*, 2010; *Koppes*, 2012].

6.3. Comparison With ^{210}Pb Measurements From Other Glacimarine Settings

[33] Many of the excess ^{210}Pb profiles from WAP and Chilean fjords, as well as those previously reported from other WAP fjords [*Harden et al*., 1992; *Domack and McClennen*, 1996], suggest sediment accumulation at a uniform rate over the past ~100 years. This is remarkable not only because the WAP has warmed exceptionally quickly and most glaciers have retreated significantly in the last century, but also because it contrasts with profiles of excess ^{210}Pb from ice proximal, temperate fjord settings. Profiles collected from multiple fjords in Alaska typically exhibit nonsteady state behavior [*Cowan et al*., 1997; *Jaeger and Nittrouer*, 1999], which for these glacier proximal settings likely indicate the greater contribution of individual sediment delivery events, and temporal changes in their frequency and magnitude. The low values of excess activity for these profiles suggest that either particles settle through the water column too quickly to scavenge ^{210}Pb or sediment is delivered near the bed as submarine gravity flows [*Jaeger and Nittrouer*, 1999]. Either scenario is consistent with the rapid deposition of sediment, which is known to occur in these Alaskan fjords at seasonal rates up to 9 cm d^{-1} and annual rates of at least 9 m yr^{-1} near the terminus [e.g., Molnia, 1983; *Cowan and Powell*, 1991]. Where ^{210}Pb-derived rates can be calculated near temperate glaciers, they confirm rapid accumulation at least 2 orders of magnitude greater than ice proximal accumulation rates in subpolar fjords (Figure 10). In such ice proximal, temperate regions typically characterized by nonsteady and rapid sediment accumulation, shorter-lived isotopes such as ^{234}Th are generally more useful in quantifying accumulation rates [e.g., *Jaeger and Nittrouer*, 1999]; however, ^{210}Pb geochronology provides a considerably useful means for interpreting sedimentary processes in these environments, as well as for determining accumulation rates in more ice distal regions in temperate settings, such as the continental shelf off the southern coast of Alaska [*Jaeger et al*., 1998], and in subpolar glacimarine settings [e.g., *Smith et al*., 2002; *Szczucinski et al*., 2009].

[34] Unlike the patterns observed in ^{210}Pb profiles from ice proximal locations in temperate fjords, the steady accumulation profiles observed in most of the cores shown here resemble profiles collected in other subpolar fjords, as well as in temperate, ice distal settings. For example, most ^{210}Pb measurements from subpolar fjords in east Greenland and Svalbard indicate steady sediment accumulation rates of 1 to 10 mm yr^{-1} (Figure 10) [*Smith et al*., 2002; *Szczucinski et al*., 2009; *Andresen et al*., 2011], which encompass the rates observed along the WAP and South Shetland Islands in this and previous studies [*Harden et al*., 1992; *Domack and McClennen*, 1996]. In addition, the more ice distal regions of the outer Alaskan fjords and the adjacent continental shelf experience uniform accumulation at rates of ~1–2 cm yr^{-1} (Figure 10) [*Cowan et al*., 1997; *Jaeger et al*., 1998]. The similarity between sediment accumulation patterns and rates in the distal regions of temperate fjords and the proximal areas of subpolar fjords suggests that both settings receive glacially derived sediment continuously with infrequent "events" when averaged over typical sampling intervals of 5 cm, which correspond to periods of 50 to 5 years, respectively, for accumulation rates of 1 to 10 mm yr^{-1}. On temperate shelves fed with glacial sediments, accumulation tends to be rather steady because of the considerable distance to the sediment source, which reduces accumulation rates, attenuates event signals, and increases the averaging time for ^{210}Pb; in addition, the more temporally uniform accumulation reflects input from multiple glaciers and mixing due to postdepositional transport on the shelf. In ice proximal subpolar settings, accumulation also tends to be steady; this is presumed to be due to the long averaging time for ^{210}Pb activities that correspond to the slow accumulation, as well as the rare and spatially limited occurrence of large depositional events due to the relative dearth of meltwater.

[35] From temperate to polar settings, ^{210}Pb-derived accumulation in ice proximal settings (~5 km from modern ice front) slows by more than 2 orders of magnitude (Figure 10) [*Harden et al*., 1992; *Domack and McClennen*, 1996; *Cowan et al*., 1997; *Smith et al*., 2002; *Szczucinski et al*., 2009; *Andresen et al*., 2011]. Regardless of the magnitude of ice proximal accumulation, the general decrease in accumulation rate with distance from the glacial sediment source within individual temperate, subpolar, and polar fjords is widely recognized in ^{210}Pb data [*Cowan et al*., 1997; *Gilbert and Domack*, 2003; *Szczucinski et al*., 2009; *Andresen et al*., 2011] and in data representing both longer and shorter time scales derived with ^{14}C dating and sediment traps, respectively [e.g., *Cowan and Powell*, 1991, Figure 7; *Gilbert et al*., 1998, Figure 13; *Jaeger and Nittrouer*, 1999, Figure 10; *Szczucinski and Zajaczkowski*, 2012, Figure 8b]. However, the compiled data from various fjords, even when within the same climatic regime, do not reflect this well-documented pattern (Figure 10) [e.g., *Harden et al*., 1992; *Smith et al*., 2002], presumably due

to large interfjord differences in the factors that control sediment production rates (e.g., catchment size, lithology, joint density, geometry, ice flux); these are currently under study.

7. Conclusions

[36] Herein we presented ^{210}Pb-derived rates of modern sediment accumulation from 21 cores collected in 12 bays and fjords spanning from 50°S to 65°S. In 15 of these 21 cores, profiles of excess ^{210}Pb indicate relatively constant rates of sediment accumulation over approximately the past century, despite the coincident rapid warming, increase in the frequency of surface melting events, and considerable glacier retreat in this region [e.g., *Vaughan et al*., 2003; *Cook et al*., 2005; *Abram et al*., 2013]. Accumulation rates increase markedly from fjords along the South Shetland Islands and WAP (~1–7 mm/yr^{-1}) to Chilean fjords (~10–20 mm/yr^{-1}), and this increase highlights the role of a warmer and wetter climate in southern Chile for accelerating glacial motion and the production and transfer of sediment. In contrast with sediment cores from the WAP that show steady accumulation, ^{210}Pb records from the South Shetland Islands show that sediment accumulation accelerated over the last few decades. Increasing air temperatures and precipitation events likely generated more vigorous periglacial weathering, mass wasting, and increased volumes of meltwater, which resulted in the delivery of more sediment-laden meltwater to fjords as the region shifted toward temperate conditions. With additional warming and meltwater production, we expect fjord sediment accumulation rates to increase in the subpolar region of the Antarctic Peninsula, which would likely impact the pelagic and benthic communities [e.g., *Dierssen et al*., 2002].

[37] The relatively large and temporally variable rates of sediment accumulation in the Chilean records resemble those in temperate Alaskan fjords; they all, presumably, reflect the role of meltwater in the sporadic delivery of sediment to ice proximal fjord settings. The lower accumulation rates in the majority of subpolar fjords presented here are similar to rates in ice distal settings of temperate fjords, because of the limited supply of terrigenous material in both settings and tendency for "events" to be smoothed when averaged over a typical 5 cm sampling interval. We infer that the sediments accumulate steadily in both settings for different reasons. In the ice distal areas of temperate fjords, accumulation is relatively steady because inputs from multiple glaciers average out and attenuate the signal from single sedimentation events, and moreover, deposited sediments are mixed due to transport on the shelf. In contrast, subpolar fjord accumulation is relatively steady because it is rarely interrupted by substantial delivery of sediment-laden meltwater from the subglacial hydraulic system, presumably because melt generated at the glacier surface seldom reaches deep into subpolar glaciers despite the recent increase in surface melt events. We conclude that the steady nature of accumulation in subpolar fjords experiencing rapid warming reflects counteracting processes; a temporal increase in meltwater production accelerates the rate of sediment delivered to down-fjord sites, while terminus retreat increases the distance between the sediment source and down-fjord coring sites.

[38] **Acknowledgments.** We thank C. Landowski, J. Berquist, and T. Drexler for assistance in the field and laboratory, and the officers, crew, and scientists who sailed on the RV/IB *Palm*er during NBP0505 and NBP0703. This work was funded by National Science Foundation Office of Polar Programs grants NSF/OPP 03–38137 to J. Anderson and J. Wellner and grant NSF/OPP 03–38371 to B. Hallet. K. Boldt was funded by a NDSEG graduate fellowship. Thoughtful reviews from T. Pratt, R. Gilbert, and two anonymous reviewers significantly improved this manuscript.

References

Abram, N. J., R. Mulvaney, E. W. Wolff, J. Triest, S. Kipfstuhl, L. D. Trusel, F. Vimeux, L. Fleet, and C. Arrowsmith (2013), Acceleration of snow melt in an Antarctic Peninsula ice core during the twentieth century, *Nat. Geosci.*, *6*(5), 404–411, doi:10.1038/ngeo1787.

Anderson, J. B., and E. W. Domack (1991), Foreward, in *Glacial Marine Sedimentation: Paleoclimatic Significance*, edited by J. B. Anderson and G. M. Ashley, pp. v–viii, Geological Society of America, Boulder, CO.

Anderson, J., S. Shipp, A. Lowe, J. S. Wellner, and A. B. Mosola (2002), The Antarctic Ice Sheet during the Last Glacial Maximum and its subsequent retreat history: A review, *Quat. Sci. Rev.*, *21*, 49–70.

Anderson, R. S., S. P. Anderson, K. R. MacGregor, E. D. Waddington, S. O'Neel, C. A. Riihimaki, and M. G. Loso (2004), Strong feedbacks between hydrology and sliding of a small alpine glacier, *J. Geophys. Res.*, *109*, F03005, doi:10.1029/2004JF000120.

Andresen, C. S., et al. (2011), Rapid response of Helheim Glacier in Greenland to climate variability over the past century, *Nat. Geosci.*, *5*(1), 37–41, doi:10.1038/ngeo1349.

Appleby, P. G. (2002), Chronostratigraphic techniques in recent sediments, in *Tracking Environmental Change Using Lake Sediments*, edited by W. M. Last and J. P. Smol, pp. 189–219, Kluwer Academic Publishers, Dordrecht, The Netherlands.

Bartholomew, I., P. Nienow, D. Mair, A. Hubbard, M. A. King, and A. Sole (2010), Seasonal evolution of subglacial drainage and acceleration in a Greenland outlet glacier, *Nat. Geosci.*, *3*(6), 408–411, doi:10.1038/ngeo863.

Bentley, S. J., C. A. Nittrouer, and C. K. Sommerfield (1996), Development of sedimentary strata in Eckernforde Bay, southwestern Baltic Sea, *Geo Mar. Lett.*, *16*, 148–154.

Berger, A. L., et al. (2008), Quaternary tectonic response to intensified glacial erosion in an orogenic wedge, *Nat. Geosci.*, *1*(11), 793–799, doi:10.1038/ngeo334.

Boyd, B., J. Anderson, J. Wellner, and R. Fernández (2008), The sedimentary record of glacial retreat, Marinelli Fjord, Patagonia: Regional correlations and climate ties, *Mar. Geol.*, *255*(3–4), 165–178, doi:10.1016/j.margeo.2008.09.001.

Cook, A., A. Fox, D. Vaughan, and J. Ferrigno (2005), Retreating glacier fronts on the Antarctic Peninsula over the past half-century, *Science*, *308*(5721), 541.

Cowan, E. A., and R. D. Powell (1991), Ice-proximal sediment accumulation rates in a temperate glacial fjord, southeastern Alaska, in *Glacial Marine Sedimentation: Paleoclimatic Significance*, edited by J. B. Anderson and G. M. Ashley, pp. 61–73, Geological Society of America, Boulder, CO.

Cowan, E. A., J. Cai, R. D. Powell, J. D. Clark, and J. N. Pitcher (1997), Temperate glacimarine varves: An example from Disenchantment Bay, southern Alaska, *J. Sediment. Res.*, *67*(3), 536–549.

Cowan, E. A., K. C. Seramur, R. D. Powell, B. A. Willems, S. P. S. Gulick, and J. M. Jaeger (2010), Fjords as temporary sediment traps: History of glacial erosion and deposition in Muir Inlet, Glacier Bay National Park, southeastern Alaska, *Geol. Soc. Am. Bull.*, *122*(7–8), 1067–1080, doi:10.1130/B26595.1.

Cuffey, K. M., and W. S. B. Paterson (2010), *The Physics of Glaciers*, 4th ed., Elsevier, New York.

Cuffey, K. M., H. Conway, B. Hallet, A. M. Gades, and C. F. Raymond (1999), Interfacial water in polar glaciers and glacier sliding at −17°C, *Geophys. Res. Lett.*, *26*(6), 751–754, doi:10.1029/1999GL900096.

DaSilva, J., J. Anderson, and J. Stravers (1997), Seismic facies changes along a nearly continuous 24° latitudinal transect: The fjords of Chile and the northern Antarctic Peninsula, *Mar. Geol.*, *143*, 103–123.

Degeest, A. L., B. L. Mullenbach, P. Puig, C. A. Nittrouer, T. M. Drexler, X. Durrieu de Madron, and D. L. Orange (2008), Sediment accumulation in the western Gulf of Lions, France: The role of Cap de Creus Canyon in linking shelf and slope sediment dispersal systems, *Cont. Shelf Res.*, *28*(15), 2031–2047, doi:10.1016/j.csr.2008.02.008.

DeMaster, D. J., B. A. McKee, C. A. Nittrouer, Q. Jiangchu, and C. Guodong (1985), Rates of sediment accumulation and particle reworking based on radiochemical measurements from continental shelf deposits in the East China Sea, *Cont. Shelf Res.*, *4*(1–2), 143–158, doi:10.1016/0278-4343(85)90026-3.

DeMaster, D. J., T. M. Nelson, S. L. Harden, and C. A. Nittrouer (1991), The cycling and accumulation of biogenic silica and organic carbon in Antarctic deep-sea and continental margin environments, *Mar. Chem.*, *35*(1–4), 489–502, doi:10.1016/S0304-4203(09)90039-1.

Dierssen, H. M., R. C. Smith, and M. Vernet (2002), Glacial meltwater dynamics in coastal waters west of the Antarctic Peninsula, *Proc. Natl. Acad. Sci. U. S. A.*, *99*(4), 1790–5, doi:10.1073/pnas.032206999.

Domack, E. W., and S. E. Ishman (1993), Oceanographic and physiographic controls on modern sedimentation within Antarctic fjords, *Geol. Soc. Am. Bull.*, *105*(9), 1175–1189, doi:10.1130/0016-7606(1993)105<1175.

Domack, E. W., and C. E. McClennen (1996), Accumulation of glacial marine sediments in fjords of the Antarctic Peninsula and their use as late Holocene paleoenvironmental indicators, *Antarct. Res. Ser.*, *70*, 135–154.

Domack, E., A. Leventer, R. Dunbar, F. Taylor, S. Brachfeld, and C. Sjunneskog (2001), Chronology of the Palmer Deep site, Antarctic Peninsula: A Holocene palaeoenvironmental reference for the circum-Antarctic, *The Holocene*, *11*(1), 1–9, doi:10.1191/095968301673881493.

Ducklow, H. W., K. Baker, D. G. Martinson, L. B. Quetin, R. M. Ross, R. C. Smith, S. E. Stammerjohn, M. Vernet, and W. Fraser (2007), Marine pelagic ecosystems: The West Antarctic Peninsula, *Philos. Trans. R. Soc., B: Biological Sciences*, *362*(1477), 67–94, doi:10.1098/rstb.2006.1955.

Dukat, D. A., and S. A. Kuehl (1995), Non-steady-state ^{210}Pb flux and the use of ^{228}Ra/^{226}Ra as a geochronometer on the Amazon continental shelf, *Mar. Geol.*, *125*(3–4), 329–350, doi:10.1016/0025-3227(95)00018-T.

Dunbar, R. B., J. B. Anderson, and E. W. Domack (1985), Oceanographic influences on sedimentation along the Antarctic continental shelf, in *Oceanology of the Antarctic Continental Shelf*, Antarctic Research Series, vol. 43, edited by S. S. Jacobs, pp. 291–312, AGU, Washington, D. C.

Egholm, D. L., S. B. Nielsen, V. K. Pedersen, and J.-E. Lesemann (2009), Glacial effects limiting mountain height, *Nature*, *460*(7257), 884–887, doi:10.1038/nature08263.

Elverhøi, A., R. L. B. Hooke, and A. Solheim (1998), Late Cenozoic erosion and sediment yield from the Svalbard–Barents Sea region: Implications for understanding erosion of glacierized basins, *Quat. Sci. Rev.*, *17*(1–3), 209–241.

Fernandez, R. A., J. B. Anderson, J. S. Wellner, and B. Hallet (2011), Timescale dependence of glacial erosion rates: A case study of Marinelli Glacier, Cordillera Darwin, southern Patagonia, *J. Geophys. Res.*, *116*, F01020,, doi:10.1029/2010JF001685.

Gilbert, R., N. Nielsen, J. R. Desloges, and M. Rasch (1998), Contrasting glacimarine sedimentary environments of two arctic fiords on Disko, West Greenland, *Mar. Geol.*, *147*(1–4), 63–83, doi:10.1016/S0025-3227(98)00008-5.

Gilbert, R., and E. W. Domack (2003), Sedimentary record of disintegrating ice shelves in a warming climate, Antarctic Peninsula, *Geochem. Geophys. Geosyst.*, *4*(4), 1038, doi:10.1029/2002GC000441.

Gilbert, R., Å. Chong, R. B. Dunbar, and E. W. Domack (2003), Sediment Trap records of glacimarine sedimentation at Müller Ice Shelf, Lallemand Fjord, Antarctic Peninsula, *Arct. Antarct. Alp. Res.*, *35*(1), 24–33, doi:10.1657/1523-0430(2003)035.

Griffith, T. W., and J. B. Anderson (1989), Climatic control of sedimentation in bays and fjords of the northern Antarctic Peninsula, *Mar. Geol.*, *85*(2–4), 181–204.

Hallet, B. (1996), Glacial quarrying: A simple theoretical model, *Ann. Glaciol.*, *22*, 1–8.

Hallet, B., L. Hunter, and J. Bogen (1996), Rates of erosion and sediment evacuation by glaciers: A review of field data and their implications, *Global Planet. Change*, *12*(1–4), 213–235, doi:10.1016/0921-8181(95)00021-6.

Harden, S. L., D. DeMaster, and C. Nittrouer (1992), Developing sediment geochronologies for high-latitude continental shelf deposits: A radiochemical approach, *Mar. Geol.*, *103*, 69–97.

Harris, P., E. Domack, P. Manley, and R. Gilbert (1999), Andvord drift: A new type of inner shelf, glacial marine deposystem from the Antarctic Peninsula, *Geology*, *27*, 683–686, doi:10.1130/0091-7613(1999)027<0683.

Hay, W., J. L. I. Sloan, and C. N. Wold (1988), Mass/age distribution and composition of sediments on the ocean floor and the global rate of sediment subduction, *J. Geophys. Res.*, *93*(B12), 14,933–14,940.

Holland, M. M., and C. M. Bitz (2003), Polar amplification of climate change in coupled models, *Clim. Dyn.*, *21*(3–4), 221–232, doi:10.1007/s00382-003-0332-6.

Hooke, R., and A. Elverhøi (1996), Sediment flux from a fjord during glacial periods Isfjorden, Spitsbergen, *Global Planet. Change*, *12*, 237–249.

Hulton, N., R. Purves, R. McCulloch, D. E. Sugden, and M. J. Bentley (2002), The last glacial maximum and deglaciation in southern South America, *Quat. Sci. Rev.*, *21*, 233–241.

Humphrey, N. F., and C. Raymond (1994), Hydrology, erosion and sediment production in a surging glacier: Variegated Glacier, Alaska, 1982–83, *J. Glaciol.*, *40*(136), 539–552.

Hunter, L. E., R. D. Powell, and D. E. Lawson (1996), Flux of debris transported by ice at three Alaskan tidewater glaciers, *J. Glaciol.*, *42*(140), 123–135.

Iken, A., and R. A. Bindschadler (1986), Combined measurements of subglacial water pressure and surface velocity of Findelengletscher Switzerland: Conclusions about drainage system and sliding mechanism, *J. Glaciol.*, *32*, 101–119.

Iverson, N. R. (2012), A theory of glacial quarrying for landscape evolution models, *Geology*, *40*(8), 679–682, doi:10.1130/G33079.1.

Jaeger, J. M., and C. A. Nittrouer (1999), Sediment deposition in an Alaskan fjord: Controls on the formation and preservation of sedimentary structures in Icy Bay, *J. Sediment. Res.*, *69*(5), 1011–1026.

Jaeger, J. M., C. A. Nittrouer, N. D. Scott, and J. D. Milliman (1998), Sediment accumulation along a glacially impacted mountainous coastline: North-east Gulf of Alaska, *Basin Res.*, *10*, 155–173.

King, J. C., J. Turner, G. J. Marshall, W. M. Connolley, and T. A. Lachlan-Cope (2003), Antarctic Peninsula climate variability and its causes revealed by analysis of instrumental records, in *Antarctic Peninsula Climate Variability*, Antarctic Research Series, vol. 79, edited by E. Domack et al., pp. 17–30, AGU, Washington, D. C.

Koppes, M. N. (2007), Glacier erosion and response to climate, from Alaska to Patagonia, PhD Thesis, Dept. of Earth and Space Sci., Univ. of Washington, Seattle, WA, USA.

Koppes, M. N. (2012), Climate-driven variability of glacier erosion and its impact on mountain evolution, Abstract EP012-0107 presented at 2012 Fall Meeting, AGU, San Francisco, Calif., 3–7 Dec.

Koppes, M. N., and B. Hallet (2002), Influence of rapid glacial retreat on the rate of erosion by tidewater glaciers, *Geology*, *30*(1), 47, doi:10.1130/0091-7613(2002)030<0047:IORGRO>2.0.CO;2.

Koppes, M. N., and B. Hallet (2006), Erosion rates during rapid deglaciation in Icy Bay, Alaska, *J. Geophys. Res.*, *111*, F02023, doi:10.1029/2005JF000349.

Koppes, M. N., and B. Hallet (2010), Glacier erosional response to transient climate, Abstract EP52A-03 presented at 2010 Fall Meeting, AGU, San Francisco, Calif., 13–17 Dec.

Koppes, M. N., and D. R. Montgomery (2009), The relative efficacy of fluvial and glacial erosion over modern to orogenic timescales, *Nat. Geosci.*, *2*(9), 644–647, doi:10.1038/ngoe616.

Koppes, M. N., B. Hallet, and J. B. Anderson (2009), Synchronous acceleration of ice loss and glacial erosion, Glaciar Marinelli, Chilean Tierra del Fuego, *J. Glaciol.*, *55*(190), 207–220, doi:10.3189/002214309788608796.

Koppes, M. N., R. Sylwester, A. Rivera, and B. Hallet (2010), Variations in sediment yield over the advance and retreat of a calving glacier, Laguna San Rafael, North Patagonian Icefield, *Quat. Res.*, *73*(1), 84–95, doi:10.1016/j.yqres.2009.07.006.

Kuehl, S. A., T. M. Hariu, and W. S. Moore (1989), Shelf sedimentation off the Ganges-Brahmaputra system: Evidence for sediment bypassing to the Bengal fan, *Geology*, *17*(12), 1132–1135.

Ledford-Hoffman, P., D. DeMaster, and C. Nittrouer (1986), Biogenic-silica accumulation in the Ross Sea and the importance of Antarctic continental-shelf deposits in the marine silica budget, *Geochim. Cosmochim. Acta*, *50*, 2099–2110.

Leventer, A., E. W. Domack, S. E. Ishman, S. Brachfeld, C. E. McClennen, and P. Manley (1996), Productivity cycles of 200–300 years in the Antarctic Peninsula region: Understanding linkages among the sun, atmosphere, oceans, sea ice, and biota, *Geol. Soc. Am. Bull.*, *108*, 1626–1644, doi:10.1130/0016-7606(1996)108<1626.

Majewski, W., J. S. Wellner, W. Szczucinski, and J. B. Anderson (2012), Holocene oceanographic and glacial changes recorded in Maxwell Bay, West Antarctica, *Mar. Geol.*, *326*, 67–79, doi:10.1016/j.margeo.2012.08.009.

McCave, I. N., R. J. Bryant, H. F. Cook, and C. A. Coughanowr (1986), Evaluation of a laser-diffraction-size analyzer for use with natural sediments, *J. Sediment. Petrol.*, *56*, 561–564.

McClintic, M. A., D. J. DeMaster, C. J. Thomas, and C. R. Smith (2008), Testing the FOODBANCS hypothesis: Seasonal variations in near-bottom particle flux, bioturbation intensity, and deposit feeding based on ^{234}Th measurements, *Deep Sea Res. Part II: Topical Studies in Oceanography*, *55*(22–23), 2425–2437, doi:10.1016/j.dsr2.2008.06.003.

Michalchuk, B. R., J. B. Anderson, J. S. Wellner, P. L. Manley, W. Majewski, and S. Bohaty (2009), Holocene climate and glacial history of the northeastern Antarctic Peninsula: The marine sedimentary record from a long SHALDRIL core, *Quat. Sci. Rev.*, *28*(27–28), 3049–3065, doi:10.1016/j.quascirev.2009.08.012.

Milliken, K. T., J. B. Anderson, J. S. Wellner, S. M. Bohaty, and P. L. Manley (2009), High-resolution Holocene climate record from Maxwell Bay, South Shetland Islands, Antarctica, *Geol. Soc. Am. Bull.*, *121*(11–12), 1711–1725, doi:10.1130/B26478.1.

Molnia, B. (1983), Subarctic glacial-marine sedimentation: A model, in *Glacial-Marine Sedimentation*, edited by B. Molnia, pp. 95–477, Plenum Press, New York.

Monien, P., B. Schnetger, H.-J. Brumsack, H. C. Hass, and G. Kuhn (2011), A geochemical record of late Holocene palaeoenvironmental changes at King George Island (maritime Antarctica), *Antarct. Sci.*, *23*, 255–267, doi:10.1017/S095410201100006X.

Mullenbach, B. L., and C. A. Nittrouer (2000), Rapid deposition of fluvial sediment in the Eel Canyon, northern California, *Cont. Shelf Res.*, *20*(16), 2191–2212, doi:10.1016/S0278-4343(00)00067-4.

Nittrouer, C., R. Sternberg, and R. Carpenter (1979), The use of Pb-210 geochronology as a sedimentological tool: Application to the Washington continental shelf, *Mar. Geol.*, *31*, 297–316.

Nittrouer, C. A., D. DeMaster, B. A. McKee, N. H. Cutshall, and I. L. Larsen (1984), The effect of sediment mixing on Pb-210 accumulation rates for the Washington continental shelf, *Mar. Geol.*, *54*, 201–221.

Palinkas, C. M., and C. A. Nittrouer (2006), Clinoform sedimentation along the Apennine shelf, Adriatic Sea, *Mar. Geol.*, *234*, 245–260.

Powell, R. D., and B. F. Molnia (1989), Glacimarine sedimentary processes, facies and morphology of the south-southeast Alaska shelf and fjords, *Mar. Geol.*, *85*(2–4), 359–390.

Powell, R. D., M. Dawber, J. N. McInnes, and A. R. Pyne (1996), Observations of the grounding-line area at a floating glacier terminus, *Ann. Glaciol.*, *22*, 217–223.

Pritchard, H. D., and D. G. Vaughan (2007), Widespread acceleration of tidewater glaciers on the Antarctic Peninsula, *J. Geophys. Res.*, *112*, F03S29, doi:10.1029/2006JF000597.

Rau, F., and M. Braun (2002), The regional distribution of the dry-snow zone on the Antarctic Peninsula north of 70S, *Ann. Glaciol.*, *34*, 95–100.

Reynolds, J. M. (1981), The distribution of mean annual temperatures in the Antarctic Peninsula, *Br. Antarct. Surv. Bull.*, *54*(1), 123–133.

Riihimaki, C. A., K. R. MacGregor, R. S. Anderson, S. P. Anderson, and M. G. Loso (2005), Sediment evacuation and glacial erosion rates at a small alpine glacier, *J. Geophys. Res.*, *110*, F03003, doi:10.1029/2004JF000189.

Rückamp, M., and N. Blindow (2011), King George Island ice cap geometry updated with airborne GPR measurements, *Earth Syst. Sci. Data Discuss.*, *4*(1), 123–139, doi:10.5194/essdd-4-123-2011.

Simms, A. R., K. T. Milliken, J. B. Anderson, and J. S. Wellner (2011), The marine record of deglaciation of the South Shetland Islands, Antarctica since the Last Glacial Maximum, *Quat. Sci. Rev.*, *30*(13–14), 1583–1601, doi:10.1016/j.quascirev.2011.03.018.

Smith, L., C. Alexander, and A. Jennings (2002), Accumulation in east Greenland fjords and on the continental shelves adjacent to the Denmark Strait over the last century based on ^{210}Pb geochronology, *Arctic*, *55*(2), 109–122.

Sommerfield, C. K., and C. A. Nittrouer (1999), Modern accumulation rates and a sediment budget for the Eel shelf: A flood-dominated depositional environment, *Mar. Geol.*, *154*, 227–241.

Syvitski, J. P. M. (1991), Towards an understanding of sediment deposition on glaciated continental shelves, *Cont. Shelf Res.*, *11*, 897–937.

Szczucinski, W., and M. Zajaczkowski (2012), Factors controlling downward fluxes of particulate matter in glacier-contact and non-glacier contact settings in a subpolar fjord (Billefjorden, Svalbard), in *Sediments, Morphology and Sedimentary Processes on Continental Shelves*, International Association of Sedimentologists, vol. 44, edited by M. Z. Li, C. R. Sherwood, and P. R. Hill, pp. 369–386, Wiley-Blackwell, Oxford, UK.

Szczucinski, W., M. Zajaczkowski, and J. Scholten (2009), Sediment accumulation rates in subpolar fjords—Impact of post-Little Ice Age glaciers retreat, Billefjorden, Svalbard, *Estuarine Coastal Shelf Sci.*, *85*(3), 345–356, doi:10.1016/j.ecss.2009.08.021.

Thomson, S. N., M. T. Brandon, J. H. Tomkin, P. W. Reiners, C. Vásquez, and N. J. Wilson (2010), Glaciation as a destructive and constructive control on mountain building, *Nature*, *467*(7313), 313–7, doi:10.1038/nature09365.

Turner, J., S. R. Colwell, and S. Harangozo (1997), Variability of precipitation over the coastal western Antarctic Peninsula from synoptic observations, *J. Geophys. Res.*, *102*(D12), 13,999–14,007, doi:10.1029/96JD03359.

Turner, J., T. Lachlan-Cope, G. Marshall, E. Morris, R. Mulvaney, and W. Winter (2002), Spatial variability of Antarctic Peninsula net surface mass balance, *J. Geophys. Res.*, *107*(D13), 4173, doi:10.1029/2001JD000755.

Turner, J., T. Lachlan-Cope, S. Colwell, and G. J. Marshall (2005), A positive trend in western Antarctic Peninsula precipitation over the last 50 years reflecting regional and Antarctic-wide atmospheric circulation changes, *Ann. Glaciol.*, *41*(1), 85–91.

Vaughan, D. G., G. J. Marshall, W. M. Connolley, C. Parkinson, R. Mulvaney, D. A. Hodgson, J. C. King, C. J. Pudsey, and J. Turner (2003), Recent rapid regional climate warming on the Antarctic Peninsula, *Clim. Change*, *60*(3), 243–274.

Vorren, T. O., G. Richardsen, S.-M. Knutsen, and E. Henriksen (1991), Cenozoic erosion and sedimentation in the western Barents Sea, *Mar. Pet. Geol.*, *8*, 317–340.

Yoon, H., B. Park, and E. Domack (1998), Distribution and dispersal pattern of suspended particulate matter in Maxwell Bay and its tributary Marian Cove, in the South Shetland Islands, West Antarctica, *Mar. Geol.*, *152*, 261–275.

Yoon, H., B. Park, and Y. Kim (2000), Glaciomarine sedimentation and its paleoceanographic implications along the fjord margins in the South Shetland Islands, Antarctica during the last 6000 years, *Palaeogeogr. Palaeoclimatol. Palaeoecol.*, *157*, 189–211.

Yoon, H. I., K.-C. Yoo, Y.-S. Bak, H. S. Lim, Y. Kim, and J. I. Lee (2010), Late Holocene cyclic glaciomarine sedimentation in a subpolar fjord of the South Shetland Islands, Antarctica, and its paleoceanographic significance: Sedimentological, geochemical, and paleontological evidence, *Geol. Soc. Am. Bull.*, *122*(7–8), 1298–1307, doi:10.1130/B30178.1.

Zhang, P., P. Molnar, and W. R. Downs (2001), Increased sedimentation rates and grain sizes 2–4 Myr ago due to the influence of climate change on erosion rates, *Nature*, *410*(6831), 891–7, doi:10.1038/35073504.